COMPUTATIONAL MECHANOBIOLOGY OF FILAMENTOUS PROTEINS: ALPHA-HELICAL COILED COILS AND F-ACTIN

by

Osman N. Yogurtcu

A dissertation submitted to The Johns Hopkins University in conformity with the requirements for the degree of Doctor of Philosophy.

Baltimore, Maryland

October, 2013

© Osman N. Yogurtcu 2013

All rights reserved

Abstract

This dissertation sits at the intersection of mechanics and biology. Specifically, we devise mesoscopic mechanochemical models to study biofilaments, very ubiquitous cellular protein structures. Since they undergo functional bending, twisting, buckling and stretching motions, understanding the mechanical response of biofilaments is crucial for a correct description of the conformational states of these proteins. Our models contribute to the better understanding of the nonlinearities in the mechanical response of biofilaments to the environmental perturbations, without resorting to computationally costly full atomistic simulations. Two important filamentous structures coiled-coil and actin make up the main concentration of our work. Coiled coils are a rope-like protein motif formed by two or more alpha helices. The energetic of a coiled coil involves a competition between elastic deformation and hydrophobic interaction of residues of each helix. The model treats alpha helices as elastic rods where each rod interacts with another exclusively through beads representing the hydrophobic residues. We validate our model using steered molecular dynamics simulations and compare it with continuum thin rod model. We analyze the bending, buckling

and twisting behavior of coiled coil molecules of various lengths and conclude that a coiled coil molecule cannot be fully characterized by a simple single-parameter mechanical model. The second filamentous biological structure we study is filamentous actin, F-actin, which is an important player in eukaryotic cellular processes including motility, morphogenesis, and mechanosensation. Actin monomer, G-actin, polymerizes to form F-actin. G-actin is an ATP hydrolase and at any time it is bound to either an ATP or ADP molecule. Mechanical and chemical properties of actin filaments are strongly coupled to each other through the bound nucleotide type. In our model of F-actin, each monomer is treated as a spherical particle with a bound molecule identity. The particles are connected by a set of springs with changing mechanical properties that depend on the bound molecule. Using this model, we study and explain the behavior of actin filaments under various external mechanical stimuli introduced by actin binding proteins. Finally, we discuss the coupling of monomer chemical state changes to the global mechanical response of actin.

Dissertation Advisor: Dr. Sean X. Sun

Dissertation Readers:

Professor, Dr. Denis Wirtz, Chemical and Biomolecular Engineering

Associate Professor, Dr. Sean X. Sun, Mechanical Engineering

Associate Professor, Dr. Noah Cowan, Mechanical Engineering

Acknowledgments

In essence, this thesis is a thirty-year-long collaborative product of my family, professors, friends and myself. I would like to take this opportunity to thank them all starting with my parents Bedil and Mahmut Yogurtcu who performed the very first collaboration and who never stopped believing in me. I also thank the members of my extended family and my Bosnian family in Maryland; Salko, Vildana and Vedrana Hodzic who eased my homesickness.

Secondly, I thank all my professors. From Istanbul; Drs. Burak Erman, Engin Erzin, Ozlem Keskin, Alper Erdogan, Alper Demir, Turkan Haliloglu, Metin Turkay and Attilla Gursoy have been great role-models for me and made my career decision to be a scientist very easy. At Hopkins; it has been a great pleasure to know Drs. Sean Sun, Denis Wirtz, Alexander Spector, Michael Falk, Markus Hilpert, Vincent Hilser, Richard Conn Henry, Rebecca Schulman, Jaafar El-Awady, Steven Marra, Vicky Nguyen, Omar Knio, Jeff Wang and Noah Cowan. Of course my deepest gratitude goes to Dr. Sean Sun for teaching me how to do good science and supporting me over the years. For me, he is the Richard Branson of academia. I also thank Dr. Wirtz

and Dr. Cowan for devoting their precious time to reading this thesis and being my committee members. My special thanks go to our mechanical engineering academic program administrator Mike Bernard whose helpfulness and dedication to his work is truly inspiring.

Thirdly, I thank all my friends in Baltimore from whom I learnt a lot and with whom I spent wonderful time: Jin Seob Kim, Giovanni Stracquadanio, Elisa Pappalardo, Sam Walcott, Sarita Koride, Bo Li, Fangwei Si, Hongyuan Jiang, Ben Harland, Meghan Vellotti, Mehdi Rahman, Hasan Shihab, Allen Zhang, Ismail Hameduddin, Ahmed Hussein, Ganhui Lan, Anjil Giri and Angela Jimenez. I also thank the Hopkins Turks community in Baltimore; Bilal Kerman, Recep Ozgun, Orhan Ozguner, Mert Ankarali, Ela Ankarali, Can Ceritoglu, Bora Erdemli, Sancar Adali, Metin Uyanik, Ali Yavuz Polat, Beril Gok, Aslan Yelken and Suat Yelken. I will also never forget the fun we had with the members of our very successful rock band, the Fish Closet: Alex Rhee, Daniel Tward, Elliot Greenwald and Mikhail Gorbounov.

Finally, I would like to thank God for making me meet all these fantastic personalities and for giving me the opportunity to do research at this wonderful university and to live in the greatest city in America.

Dedication

This thesis is dedicated to all the graduate students around the world, seeking knowledge and aiming to put that knowledge to work for the good of humanity.

Contents

List of Tables

List of Figures

Chapter 1

Introduction

In this chapter, we give a brief overview of mechanobiology and make an introduction to the topics that are discussed in the following chapters while providing definitions of important concepts.

1.1 Mechanics in Biology

Although maybe not very obvious at the first peek, mechanics and biology are two intertwined disciplines in all length scales. Flight of a bird, walking of a cockroach, swimming of a whale, forces generated by a muscle fiber, crawling of a cell and mechanical responses of biomolecules are all systems that can be analyzed using mechanics. For humans at the organ level, mechanical homeostasis is necessary to an individual's survival. Bones, muscles, lungs, vasculature and heart are mechanosen-

sitive organs. For example, an astronaut loses about 1% of his/her bone mass per month in a space mission due to disuse osteoporosis [1]. A simple calculation yields a 50% bone mass loss in a 5-year-long space mission! How the mechanical homeostasis is maintained in organs and tissues through cellular machinery is an active field of research. One such exemplary machinery that is found to sense and respond to environmental mechanical signals is focal adhesion complex [2]. On a focal adhesion complex, forces from the extracellular matrix are sensed and converted into chemical signals through G-proteins and this alters the behavior of the force generating modules of the cell and a mechanical response is produced [3]. Mechanics play a role in the cellular differentiation as well. Recent studies have shown that the differentiation fate of a stem cell is determined by the mechanical properties of the environment that it is planted in [4, 5]. Also, it is generally accepted that tumor cells are stiffer than their environment and this is used to detect cancerous cells in a tissue [6, 7].

The examples laid out above is an excellent source of motivation to better understand the effects of mechanics in biological systems, as this would potentially have a big impact on medicine and techonology. This dissertation aims at pushing the boundaries of knowledge on nonlinear mechanical behavior of filamentous biomolecules.

1.2 Biofilaments

Filamentous biomolecules are very common in nature and they undertake a great variety of important roles. In muscle contraction and regulation, the basic elements of a sarcomere, titin, myosin, actin, tropomyosin are filamentous molecules. Also, bacterial flagella and chemoreceptor, which are crucial to the survival of bacteria, are simply biofilaments. Biofilaments are important in reproduction as well. Tail of sperm cells are made of microtubules. In addition, the auditory and olfactory systems make use of biofilaments. Ear stereocilia contain actin filaments. Biofilaments also take roles in structural integrity of organs. Collagen, keratin and elastin are filamentous molecules. Finally, DNA is a biofilament. All these biofilaments are under constant interaction with their environment and understanding their response to mechanical signals is important.

Biofilaments are of mainly two origins, nucleic acid and amino acid. The remainder of this chapter will be devoted to biofilaments of amino acid origin in line with the focus of our current work.

1.2.1 Protein-based filaments

Amino acids are organic compunds which carry both an amine (NH_2) and a carboxylic acid (COOH) group. The characteristics of an amino acid is decided by its R side-chain group. Based on their R group, amino acids can be classified into being hy-

drophobic, hydrophillic, negatively or positively charged. Alanine, leucine, ileucine, valine, tyrosine, phenylalanine and tryptophane are hydrophobic amino acids. A protein is a polymer chain whose monomers are amino acids. Covalent bonds formed between each amino acid is called a peptide bond (Fig. 1.1A). A residue is defined as an amino acid in a polypeptide chain. Non-neighboring residues interact through intermolecular forces. These are weaker forces in comparison to the covalent bonds. Intermolecular forces in a protein come from ionic ($\sim$0.2-10kT), hydrogen bond ($\sim$1-5kT), hydrophobic ($\sim$1-5kT) and van der Waals interactions ($\sim$1-2kT) [8]. To compare, the energy of a single ATP hydrolysis releases 20kT [8]. All these mentioned chemical interactions give a protein its native conformation. Predicting the final conformation of a protein by looking at its amino acid sequence is extremely difficult. This is called the protein folding problem. Alpha helix is one of the most common substructures of a protein. Formation of alpha helices is done solely through hydrogen bonding between the i^{th} and $i + 4^{th}$ residues. This repetitive fashion of interactions results in a well defined right-handed helical geometry (see Fig.1.1B) with a typical radius of 0.23 nm. Each amino acid on an alpha helix contributes to an axial rise of about 0.15 nm. This rise corresponds to about 100° rotation along the helical axis. Hence, it takes almost 3.6 residues to complete a full circle (360°). As a result, when a full circle is complete, the total rise along the helical axis is about 0.54 nm. This is description of the pitch of an alpha helix. Mechanical properties of alpha helices are known.

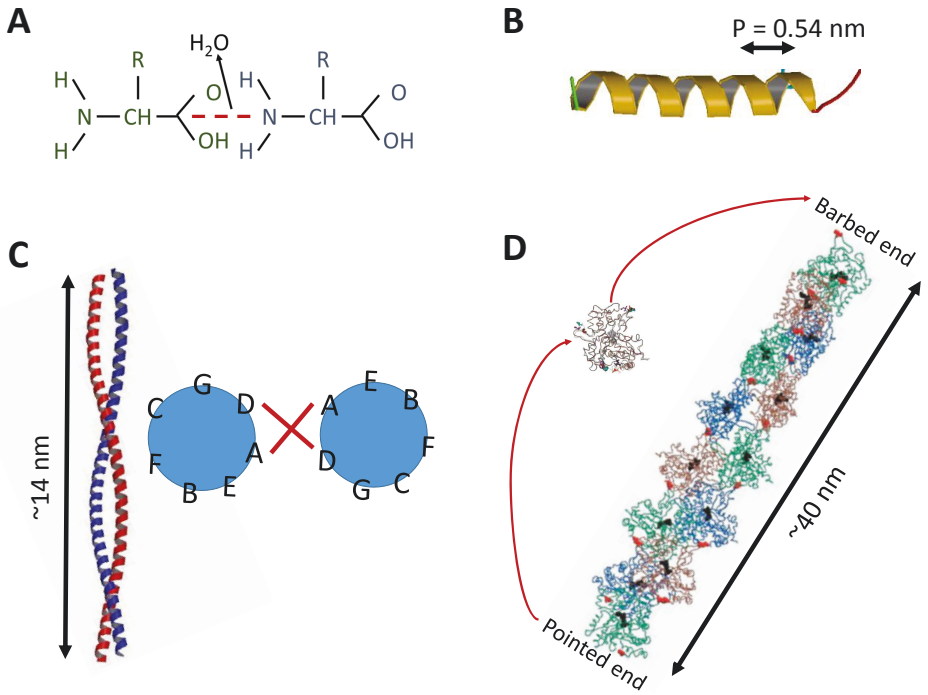

Figure 1.1: Alpha helix, coiled coil and F-actin. (A) Peptide bond formation between two amino acids yields one molecule of water. (B) Representative alpha helix (PDBID: 4J4A). Pitch of alpha helix is about 0.54 nm. (C) Cortexillin is a typical coiled coil dimer (PDBID:1D7M). Shown alongside is a representation of the heptad repeat. (D) Adapted from [9]. F-actin is a polar filament of helical pitch 72 nm. Polymerization happens preferably at the barbed (+) end and depolymerization preferably at the pointed (-) end.

1.2.2 Coiled Coil

The hydrophobic interactions of two or more alpha helices give rise to a helical coiled coil structure. These hydrophobic interactions are in general follow a seven-unit repeat pattern called a heptad repeat (Fig. 1.1C). In this repeat unit residues on a single helix are labeled "abcdefg". In a heptad repeat unit, positions a and d are hydrophobic residues. The ionic interactions between e and g residues of opposite helices provide sequence specificity to a coiled coil [10]. A coiled coil dimer has a diameter of about 2 nm [11] and pitch of 14 nm [12].

Alpha helical coiled coil motif is present in many functionally important proteins. In exocytosis, SNARE proteins provide necessary forces to perturb lipid bilayer membrane for cargo transport. Using a similar strategy, gp41 coiled coil protein leads HIV viral entry into a healthy cell. Myosin II and V have coiled coil arms. Leucine zipper, a coiled coil dimer, regulates gene expression by binding specific regions of DNA. In addition, recently, coiled coil structures have attracted a great interest in applications in material science due to their simple and easily controllable self-assembly properties [13, 14].

1.2.3 Actin

G-actin is a globular protein of an approximate radius of 6 nm and is composed of 374 residues. F-actin can be viewed as a helical polymer of G-actin monomers. Pitch

of F-actin is 72 nm and the filament diameter is about 8 nm. A cartoon representation is provided in Fig. 1.1D.

G-actin is an ATP hydrolase. Both in the monomeric and in polymerized F-actin form it carries a nucleotide (ATP or ADP). Polymerization kinetics of G-actin-ATP and G-actin-ADP is different. Polymerization of G-actin-ATP is favored over G-actin-ADP. Polymerization depends on not only the chemical state of the monomer, but also at which end the binding happens [15]. The two ends of F-actin are named as pointed end (-) and the barbed end (+). The fact that the polymerization on the pointed end is much slower than the barbed end renders F-actin a polar filament.

With more than 100 binding partners, actin is a very central protein in a eukaryotic cell. We see actin as the thin filament in muscle sarcomere. Actin is also a key constituent of the contractile ring during cell cytokinesis. Myosin walks along actin tracks to transport cargo within a cell. Finally, as a cytoskeletal protein actin provides support to a cell and is involved in cell motility through lamellipodia and filipodia.

1.2.4 Modeling in Mechanobiology

As the main focus of this thesis is biofilaments, let us now turn to modelling of biofilaments. An obvious observation about filamentous structures is their high aspect ratios. Therefore, the simplest mathematical representation that could be used to describe the geometry of a filament is a plane curve. While this description is reasonable from a macroscopic perspective, a helix equation may be a more natural

representation as most of the biofilaments are in helical conformation. A right-handed helix h(q) of height $\frac{pQ}{2\pi}$ and radius r can be written as a parametric equation of q as follows:

$$h(q) \rightarrow (r\cos(q), r\sin(q), \frac{p}{2\pi}q),\ q\epsilon[0, Q] \tag{1.1}$$

In Equation 1.1, p is the pitch of the helix. The pitch can be defined as the distance of translation performed by the helix along the helical axis, when it is rotated by 2π along the axis (see Fig.1.1B).

Biofilaments are under constant external perturbations such as bending, twisting and stretching. Mathematical description of such deformations is needed. For this we get help from the differential geometry of curves. Let us start by finding the arc length of the example helix of Equation 1.1. The arc length L of helix h(q) is found by the following integration

$$L = \int_0^Q dq \sqrt{\left(\frac{\partial x}{\partial q}\right)^2 + \left(\frac{\partial y}{\partial q}\right)^2 + \left(\frac{\partial z}{\partial q}\right)^2}$$

We can write the above equation in terms of the tangent vector to the curve

$$L = \int_0^Q dq \left\| \frac{dh}{dq} \right\|$$

The arc length L of the example helix is then

$$L = \int_0^Q dq \left\| (-r\sin(q), r\cos(q), \frac{p}{2\pi}) \right\| = Q\sqrt{r^2 + \left(\frac{p}{2\pi}\right)^2}$$

The parameterization of our curve is arbitrary. We can re-parameterize our helix using the arc length argument s using the following relation and replacing q in Equation

1.1 with s:

$$\mathrm{s} = \int_0^{\mathrm{q}} \mathrm{dq} \left\| \frac{\mathrm{dh}}{\mathrm{dq}} \right\| = \mathrm{q}\sqrt{\mathrm{r}^2 + \left(\frac{\mathrm{p}}{2\pi}\right)^2}$$

$$\mathrm{h(s)} = (\mathrm{r}\cos\left(\frac{\mathrm{s}}{\sqrt{\mathrm{r}^2 + \left(\frac{\mathrm{p}}{2\pi}\right)^2}}\right), \mathrm{r}\sin\left(\frac{\mathrm{s}}{\sqrt{\mathrm{r}^2 + \left(\frac{\mathrm{p}}{2\pi}\right)^2}}\right), \frac{\mathrm{ps}}{2\pi\sqrt{\mathrm{r}^2 + \left(\frac{\mathrm{p}}{2\pi}\right)^2}})$$

Bending of a curve is expressed by curvature. In other words, curvature measures the amount of change in the direction of the vector tangent to the curve. In our helix example the tangent vector t can be written as a function of s.

$$\mathrm{t(s)} = \frac{\mathrm{dh}}{\mathrm{ds}}$$

We note here that t(s) is a unit vector. The amount of changes in the tangent vector is found by differentiation with respect to arc length parameter s. This gives us the curvature vector $\kappa(s)$:

$$\kappa(\mathrm{s}) = \frac{\mathrm{dt}}{\mathrm{ds}}$$

The curvature is defined as the magnitude of $\kappa(s)$. The radius of curvature is the radius of the best-fitting circle around the curve at position s and it is written as the reciprocal of $\kappa(s)$. For the helix example, the curvature is equal to:

$$\frac{\mathrm{r}}{\mathrm{r}^2 + \left(\frac{\mathrm{p}}{2\pi}\right)^2}$$

The unit normal vector n to the curve can be derived from the tangent vector as follows:

$$\mathrm{n(s)} = \frac{1}{\|\kappa\|}\frac{d\kappa}{ds}$$

By using differentiation of the dot product rule, it can be shown that the two vectors $\kappa(s)$ and n(s) are orthogonal to each other. In R^3, if we have two orthonormal vectors, we can define a new vector that is orthogonal to both constituent vectors. In our case, the third orthonormal vector is called the binormal vector (b):

$$\mathrm{b} = \mathrm{t} \times \mathrm{n}$$

Similar to the tangent vector, the variations in the binormal vector with respect to the arc length is a measure of twist of the curve. This measure is called torsion $\tau(s)$ and defined as:

$$\tau = -\mathrm{n} \cdot \frac{\mathrm{db}}{\mathrm{ds}}$$

Sign of the torsion tells us if a helix is right or left-handed. If torsion is positive, then the helix is right-handed. For the helix example, the torsion is equal to:

$$\tau = \frac{\frac{\mathrm{p}}{2\pi}}{\mathrm{r}^2 + \left(\frac{\mathrm{p}}{2\pi}\right)^2}$$

Curvature and torsion is necessary and sufficient to describe the geometry of a curve and the local deformations. The vectors t, n and b form a body attached orthonormal frame called Frenet frame, $F\{t, n, b\}$. Evolution of $F\{t, n, b\}$ is given by the solution to the Frenet-Serret equations:

$$\begin{bmatrix} \frac{dt}{ds} \\ \frac{dn}{ds} \\ \frac{db}{ds} \end{bmatrix} = \begin{bmatrix} 0 & \kappa(s) & 0 \\ -\kappa(s) & 0 & \tau(s) \\ 0 & -\tau(s) & 0 \end{bmatrix} \begin{bmatrix} t \\ n \\ b \end{bmatrix}$$

$$F(\mathrm{s}) = \Omega F(0) = \exp \begin{bmatrix} 0 & \kappa(s) & 0 \\ -\kappa(s) & 0 & \tau(s) \\ 0 & -\tau(s) & 0 \end{bmatrix} F(0)$$

where $F(0)$ is the Frenet frame at $\mathrm{s} = 0$. We note that the Ω is a skew-symmetric matrix and its exponentiation yields an orthogonal matrix. Also, when defining our $F(s)$, one would observe that the choice of vectors n and b is arbitrary so long t is the tangent vector. However, the particular choice of $F\{t, n, b\}$ results in the least number of deformation constants (in this case 2, curvature and torsion). Any other choice would yield in 3 deformation constants and these are called the generalized curvatures (ω_1, ω_2, ω_3).

To make a proper mechanical description of biofilaments, we need relevant material properties, namely elastic moduli. Using these data, biofilaments are modeled assuming they obey linear elasticity. Based on the previously described generalized curvatures and stretching we can write the total elastic energy stored on a single filament as follows:

$$\mathrm{E_f} = \frac{1}{2} \int_0^{\mathrm{l}} \mathrm{ds} \left[\frac{\mathrm{C}}{\sqrt{\mathrm{g}}} \left(\sqrt{\mathrm{g}} - 1 \right)^2 + \sum_{\mathrm{i}=1}^{3} \mathrm{A_i} \left(\omega_\mathrm{i} - \Omega_\mathrm{i} \right)^2 \right] \tag{1.2}$$

where $\mathrm{A_i}$ are generalized rigidities, C stretch modulus, Ω_i are preferred curvatures and g is a stretch metric defined as

$$\mathrm{g} = \left\| \frac{\partial \mathrm{r(s)}}{\partial \mathrm{s_0}} \right\|^2$$

where $\mathrm{s_0}$ is the relaxed arc length parameter. For a system of multifilaments and

applied external work, the total energy can be written:

$$E_t = \sum_{i=1}^{n} E_f^i + E_{int} + W_{ext} \tag{1.3}$$

where E_{int} is the total filament interaction energy and W_{ext} stands for the external work term. In order to arrive at the final conformations (the set of $\omega_i(s)$), we first discretize the geometry. Then, we minimize the total energy E_t. One observation about the total energy is that the majority of the terms in the discrete summation (except work and interaction terms) is squared. Therefore, presumably the most convenient optimization algorithm for this problem is nonlinear least squares fitting. We note that spatial discretization is not the only method to solve for the final conformations. Equation 1.3 is an energy functional of generalized curvatures and stretch metric. Using principles from variational calculus this energy can be minimized. The resulting curvatures and stretch metric functions are solutions of force and moment balance equations [16,17]. Also, one could generalize elastic filament energy equation (Eq. 1.2) to situations where coupling of stiffness in all angular and translational variables considered [18,19].

We need to emphasize that there is a critical force for any biofilament beyond which rupture occurs. During simulations these forces should be taken into account. It was experimentally observed that it takes about 15 pN to start unzipping a coiled coil dimer [20], although there is some pulling rate dependence. The rupture force for F-actin is about 600 pN [21].

For our stochastic simulations in this work we used the Gillespie algorithm. This

algorithm gives us trajectories that are good representatives of a studied stochastic system [22]. The Gillespie algorithm mainly consists of two steps. These steps are repeated until the desired probability sampling is obtained. Let's assume N neighboring states. In the first step, the possible neighboring states are discovered and the rates k_i from the current state to the neighboring states are calculated, where i runs from 1 to N. Once this is done, in the second step, using the rates, τ_i the escape time from the current state is calculated and the new destination state is decided. The net escape time from the current state is sampled from an exponential distribution as follows:

$$\tau_i = -\frac{\log r_1}{\sum_i k_i} \tag{1.4}$$

where r_1 is a uniform random variable in the interval 0 and 1. For the decision of the next state, first a uniform random number r_2 is picked from the interval 0 and 1. Then, a grid of probabilities is formed by stacking the following normalized rates from 0 to 1:

$$P_i = \frac{k_i}{\sum_i k_i}$$

Finally, the new state is decided based on where r_2 falls onto in this grid. The basic idea is that the states with higher P_i will have a higher likelihood of being chosen as the new destination state. Let us briefly walk through the pictorial example shown in Fig. 1.2. Starting from S0, there is only 3 possible escape states. Assume the algorithm picked S12 as the new state, presumably because k12 is bigger than k11 and k13. Then, at state S12 we have 4 possible destination states (S0, S24, S25 and

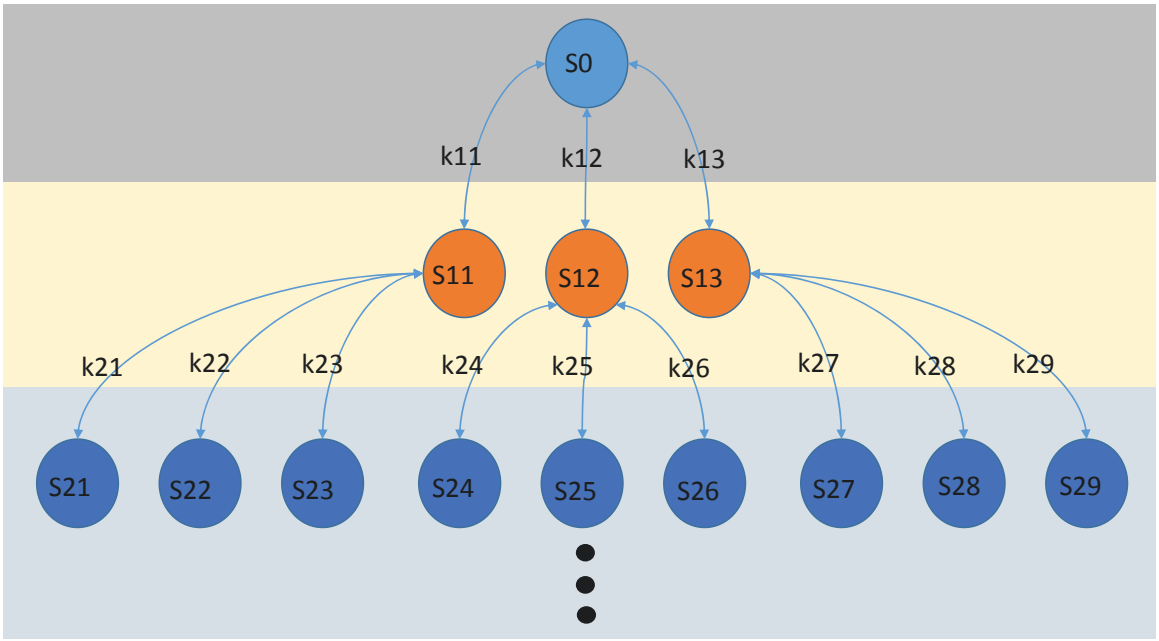

Figure 1.2: Pictorial description of a simple example Gillespie stochastic simulation. System starts at state S0. The stochastic trajectory of the system depends on the assigned rates. The net escape time from a state is picked from an exponential distribution defined by the relevant rates as discussed in the text.

S26). The following state should be chosen among these states according to their respective escape rates.

In this simple setting, we did not make a differentiation between the forward and backward rates. When running Gillespie simulations, one should make sure that the system obeys detailed balance (reversibility). This is done by imposing the following condition on forward (k_1) and backward (k_2) rates:

$$\frac{\mathrm{k_1}}{\mathrm{k_2}} = \exp\left(-\beta \triangle \mathrm{F}\right)$$

where $\triangle \mathrm{F} = \mathrm{F_1} - \mathrm{F_2}$ is the free energy difference between forward state 1 and backward state 2 and $\beta = \left(\mathrm{k_b T}\right)^{-1}$. $\mathrm{k_b}$ is the Boltzmann constant and T is the absolute temperature.

The organization of the rest of this thesis is as follows. On chapter 2, we first describe our coiled coil model and discuss our results. Then, on Chapter 3, we move on to our mechanochemical model of actin. Finally, we make a general summary of this work and lay out some possible future directions.

Chapter 2

Mechanical Response and Conformational Amplification in α-helical coiled coils

α-helical coiled coils are ubiquitous tertiary structural domains often found in mechanoproteins. Coiled coils have mechanical rigidity, and are often involved in force transmission between protein domains. While crystal structures of the coiled coil are available, limited information exists on its conformational flexibility. The role of hydrophobic interactions in determining the coiled coil conformation is not clear. In this work, we examine the mechanical responses of typical coiled coils, and build a coarse-grained mechanical model to describe the conformation of the protein. The model treats α-helices as elastic rods. Hydrophobic bonds arranged in a repeated

pattern determine the coiled coil structure. The model is compared to molecular dynamics simulations of coiled coils under force. We also estimate the effective bending and twisting persistence lengths of the coiled coil. The model allows us to examine unconventional responses of the coiled coil, including significant conformational amplification upon the binding of a small molecule. We find that the coiled coil does not behave as a simple elastic rod and shows complex nonlinear responses. These results are significant for understanding the role of coiled coil structures in chemoreceptors, motor proteins and mechanotransduction in general.

2.1 Introduction

Alpha-helical coiled coils (CC) are a common rope-like protein motif found in gene regulation [23], muscle contraction [24], molecular motors and cell signalling [25]. The number of unique CC structures identified in the Protein Data Bank is currently 941 [26]. How these ubiquitous protein motifs mechanistically contribute to diverse biological functions is not clear. In this work, we explore the conformational flexibility of the CC and develop a coarse-grained mechanical model to explain its response to external perturbations. The model captures the essential features of CC mechanics. We find that the CC does not behave as a simple rod-like structure. In some cases, dramatic amplification of local conformational changes are observed. The complex response to external loads may explain the roles of CC motifs in a variety of proteins

found in the cell.

The basic CC structure is a homodimer where residues in each α-helix contain a sequence pattern called the heptad repeat, typically denoted alphabetically as **abcdefg**. **a** and **d** are the hydrophobic residues which form the hydrophobic core that binds the helices together. Because there are 3.64 residues per turn in the α-helix, **a** and **d** residues form a helical arrangement on the surface of the α-helix. In order to maintain hydrophobic contact in the CC, the α-helices must twist and bend around each other (Fig. 2.1) in a fashion that Crick first described as Knobs-into-Holes (KiH) [27]. Other interhelical interactions are also important: **e-** and **g-**type residue interactions provide specificity to the structure [10], although they are generally weaker than **a-a** and **d-d** type interactions. Interhelical residue interactions are also the basis of larger and more complex α-helical bundles such as the recently found heptameric structure [28]. Therefore, mechanistic understanding of these α-helical bundles require quantitative models of residue side-chain interactions.

An important structural aspect of the CC that is experimentally observable is its pitch. Due to residue sequence irregularities, it is sometimes necessary to define local and global pitch values. The pitch of perfect CC homodimers is 12-14 nm. For trimeric or tetrameric structures, the upper limit of the pitch value becomes closer to 20nm [29, 30]. Several studies also have discussed how the pitch is related to α-helix properties based on geometric arguments [11,31]. Recently, Wolgemuth and Sun (WS) developed a model to relate the CC pitch to the mechanical properties of the

α-helix and the geometric pattern of hydrophobic residues [16]. The model assumed a continuous interaction between helices and treated the hydrophobic interactions as a constraint. WS showed that the CC under small deformation is rod-like, and bending and twisting stiffness of the CC can be estimated starting from the properties of the α-helices. The mechanical model opens the possibility of understanding conformational properties of the CC and how the CC responds to external forces. Several studies along these lines have appeared [32]. Using Normal Mode Analysis (NMA) and molecular dynamics (MD) simulations, bending and stretching stiffness and unfolding of a CC have been studied [33, 34]. From NMA and MD data, Lakkaraju and Hwang [35] recently suggested that conformations of longer CCs ($>$ 70nm) could be influenced by a critical buckling length longer than the persistence length. CC conformational studies have also suggested that CCs have the allosteric potential and they could be used as nanoswitches [36,37]. Additional conformational changes in the CCs such as sliding of an individual helix with respect to another was shown to have biological relevance [38,39]. In this work, we propose a simple scalable coarse-grained model for the CC and α-helical bundles. Specifically, we introduce a discrete interaction potential to model the hydrophobic contact between **a**- and **d**-type residues. We use this model to predict the mechanical response of a dimeric CC under force and compare with molecular dynamics simulation results and thin rod theory [40]. We find that the hydrophobic contacts provide both distance and angular constraints between the helices in CC. Under small forces, some of the mechanical response of

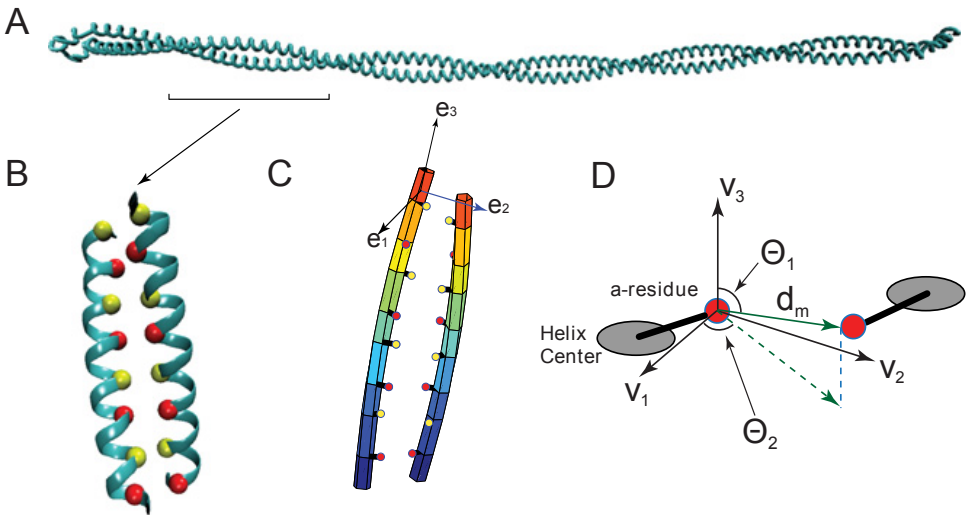

Figure 2.1: A coarse-grained mechanical model of the coiled coil. (a) Tropomyosin is a prototypical CC. Here, the crystal structure (PDBID: 2tma) is displayed. (b) A section of the coiled coil, red and yellow beads representing **a**- and **d**-type residue C_α's respectively (c) The coiled coil model represents each α-helix as a slender rod described by the rod position and local material frames $(\mathbf{e}_1(s), \mathbf{e}_2(s), \mathbf{e}_3(s))$ (Eq. 2.1). The locations of the hydrophobic residues are uniquely defined with respect to these parameters. (d) The interaction between hydrophobic residues is defined by the vector between the residues, $\mathbf{d}$, and the vector between the helix centers, $\mathbf{R}$ as shown in Eq. 2.14. For detailed definitions, see Models.

the CC can be described by a rod. However, depending on how the forces are applied, complex mechanical response is seen. In some cases, small local conformational changes in the CC is amplified by many fold over long distances. These responses can have important implications in the biological functions of the CC. The structure of this chapter is as follows: In the *Results* section we show the effects of parameter choices on the model and the response of the model CC under different external forces, then we discuss these results in *Discussion* and finally we provide a detailed description of our model in *Models*.

2.2 Models

2.2.1 Coiled Coil Kinematics

The elements of the CC model are depicted in Fig. 2.1C and 1D. Each α-helix is represented by a slender rod whose centerline is denoted as $\mathbf{r}(s)$ where s is the unstretched arclength along the helix. For points along the helix, a material frame $(\mathbf{e}_1(s), \mathbf{e}_2(s), \mathbf{e}_3(s))$ also describes the local orientation of the residues. This material frame satisfies the Frenet equations:

$$\frac{\partial \mathbf{e}_i}{\partial s} = -\sum_{j,k} \epsilon_{ijk} \mathbf{e}_j \omega_k \tag{2.1}$$

where ϵ_{ijk} is the antisymmetric tensor; $\omega_{1,2}$ are the rates of torsion and $\omega_3(s)$ is the rate of twist for the α-helix. With these parameters $(\mathbf{r}(s), \omega_1(s), \omega_2(s), \omega_3(s))$,

the unstretched configuration of the helix is completely defined. In particular, the positions of all residues can be written with respect to these quantities. We define the position of the CA atom in the m-th residue as

$$\mathbf{h}_m = \mathbf{r}(s_m) + r_0\mathbf{e}_2(s_m) \tag{2.2}$$

where s_m is the arc-length position of the m-th residue. In the unstretched helix, the helix rise per residue is 0.15nm, therefore $s_m - s_{m-1} = 0.15$ and the arclength distance between neighboring **a**-residues is 1.05nm; the radius r_0 is taken to be 0.23 nm.

Because the residues form a helical pattern in the α-helix and the helix is intrinsically straight if there are no other influences, for an isolated helix, the *instrinsic torsion and twist* of the Frenet frame is defined as

$$\begin{aligned} \Omega_1 &= \Omega_2 = 0 \\ \Omega_3 &= \frac{-\pi + \mathrm{mod}(\alpha p + \pi, 2\pi)}{p h_0} \end{aligned} \tag{2.3}$$

where $h_0 = 0.15$nm is the helical rise per residue along the centerline, p is the hydrophobic periodicity, and α is the angle between each residue.

In addition to the residue positions, it is also necessary to define the parameters specifying the hydrophobic bonds. The bond vector between m-th hydrophobic pair is

$$\mathbf{d}_m = \mathbf{h}_m - \mathbf{h}'_m \tag{2.4}$$

where the prime denotes the complimentary second helix in the CC and $\mathbf{h}'_m = \mathbf{r}'(s'_m)+$

Parameter	Symbol	Value
Intrinsic α-helical twist†	Ω_3	-0.6 nm^{-1}
Intrinsic α-helical bending torsion	$\Omega_{1,2}$	0.0
Helical rise per residue	h_0	0.15 nm
Hydrophobic periodicity	p	7
Angle between residues	α	97.7°
Helix bending persistence length	l_p	90 nm
Helix twist persistence length	l_t	45 nm
Helix stretching modulus	C	3600 pN
Hydrophobic bond length(*)	D_0	0.45nm
Hydrophobic bond elevation angle(*)	Θ_1	$\pi/2$ rad
Hydrophobic bond azimuth angle(*)	Θ_2	1.25 rad
Centerline Distance Parameter(*)	R_0	0.92nm
Energy scale	$k_{\mathrm{B}}T$	4.2 pNnm
Bond distance stiffness(*)	k_1	70 pN nm^{-1}
Bond angular stiffness(*)	k_2	200 pNnm
Hardcore repulsion parameter(*)	k_3	50 pNnm

Table 2.1: **Parameters in our coarse-grained mechanical model.** The values are for Cortexillin CC, which has $P = 12$nm. Several parameters are established properties of the CC and α-helices, and are not fitted. The fitted parameters are marked in astericks. †This value is used for the cortexillin structure used in the MD study. The intrinsic twist for typical helices such as in the leucine zipper is closer to $-0.46\mathrm{nm}^{-1}$.

$r_0\mathbf{e}'_2(s'_m)$ is the CA position of the second helix. The distance between helix centerlines is

$$\mathbf{R}_m = \mathbf{r}(s_m) - \mathbf{r}'(s'_m). \tag{2.5}$$

In our definitions, we treat the hydrophobic residues as attached rigidly to the helix material frame. Thus, the interaction potential between hydrophobic residues is, in principle, defined by the relative orientations of the helix frames $(\mathbf{e}_1(s_m), \mathbf{e}_2(s_m), \mathbf{e}_3(s_m))$ and $(\mathbf{e}'_1(s'_m), \mathbf{e}'_2(s'_m), \mathbf{e}'_3(s'_m))$. To make the definitions simple, we defined a triad centered around the m-th hydrophobic residue $(\mathbf{v}_1(m), \mathbf{v}_2(m), \mathbf{v}_3(m))$ as shown in Fig. 2.1D. The orthogonal vectors are:

$$\mathbf{v}_3(m) = \frac{1}{2}\left[\mathbf{e}_3(s_m) + \mathbf{e}'_3(s'_m)\right] \tag{2.6}$$

$$\mathbf{v}'_2(m) = \frac{\mathbf{R}_m}{|\mathbf{R}_m|} \tag{2.7}$$

$$\mathbf{v}_1(m) = \mathbf{v}'_2(m) \times \mathbf{v}_3(m) \tag{2.8}$$

$$\mathbf{v}_2(m) = \mathbf{v}_3(m) \times \mathbf{v}_1(m) \tag{2.9}$$

The orientation of the hydrophobic bond vector with respect to this frame is shown in Fig. 2.1D. We define two angles, $\theta_{1,m}$ and $\theta_{2,m}$, for the m-th residue between 2 helices as

$$\begin{aligned} \cos(\theta_{1,m}) &= \frac{\mathbf{d}_m \cdot \mathbf{v}_3(m)}{|\mathbf{d}_m|} \\ \cos(\theta_{2,m}) &= \frac{\mathbf{d}_m \cdot \mathbf{v}_1(m)}{|\mathbf{d}_m|} \end{aligned} \tag{2.10}$$

Geometrically, we see that $\theta_{1,m}$ gives the amount of sliding of a helix along the CC centerline, while $\theta_{2,m}$ is the angle of rigid body rotation of one helix with respect to the other. In our model, the conformational energy of the CC is thus completely defined by the six parameter helix configurations $(\mathbf{r}(s), \omega_1(s), \omega_2(s), \omega_3(s))$ and $(\mathbf{r}'(s'), \omega_1'(s'), \omega_2'(s'), \omega_3'(s'))$, and the hydrophobic bond parameters $(\mathbf{d}_m, \mathbf{R}_m, \theta_{1,m}, \theta_{2,m})$.

2.2.2 Coiled Coil Conformational Energy

Having defined the kinematic variables, we can write the total conformational energy of the CC as a sum of the conformational energy of the helices and bond energies of the hydrophobic contacts:

$$E = E_0[\mathbf{r}, \omega_1, \omega_2, \omega_3] + E_0[\mathbf{r}', \omega_1', \omega_2', \omega_3'] + \Delta E \tag{2.11}$$

where E_0 is the conformational energy of the α-helix; ΔE is the energy of hydrophobic contact between helices. The conformational dynamics of the α-helix has been studied. It was shown that helices are rod-like and the bending and twisting stiffness of the helices are relatively sequence independent. Thus, one may write the helix conformational energy as

$$\begin{aligned} E_0 &= \int_0^L \left[\frac{1}{2}A\left(\omega_1^2(s) + \omega_2^2(s)\right) + \frac{1}{2}B(\omega_3(s) - \Omega_3)^2\right] ds \\ &\quad + \int_0^L \frac{1}{2}\frac{C}{\sqrt{g}}(\sqrt{g} - 1)^2 ds \end{aligned} \tag{2.12}$$

where L is the length of the helix. Here, the first line represents the bending and twisting energy of the helix. The second line is the stretching energy. The amount of

stretch of the helix or the metric g is defined as

$$g = \left| \frac{\partial \mathbf{r}(s)}{\partial s_0} \right|^2 \tag{2.13}$$

where s_0 is the initial arc-length of the helix without any other influences. A and B are the bending and twist moduli of the helix, respectively. C is the stretch modulus. From molecular dynamics studies, it was shown that $A/B \approx 2$, and $A = k_{\mathrm{B}}Tl_p$ where $l_p = 90\mathrm{nm}$ is the persistence length and $k_{\mathrm{B}}T = 4.2\mathrm{pNnm}$ [41]. The parameters used in the model are described in Table 2.1.

The hydrophobic interaction energy depends on the distance between the hydrophobic residues, $d_m = |\mathbf{d}_m|$. In our model, we specify the bond energy as

$$\begin{aligned} \Delta E &= \sum_{m=1}^{N} \frac{1}{2} k_1 \left(|\mathbf{d}_m| - D_0 \right)^2 + \frac{1}{2} k_2 (\theta_{1,m} - \Theta_1)^2 \\ &\quad + \frac{1}{2} k_2 (\theta_{2,m} - \Theta_2)^2 + k_3 \exp\left[-(|\mathbf{R}_m|/R_0)^{16} \right] \end{aligned} \tag{2.14}$$

where N is the number of hydrophobic residue pairs in the CC. Interestingly, after some trial and error, we found that all four terms in the bond energies are necessary, suggesting that hydrophobic interactions between residues are complex and contain both distance and angular constraints. The first term is the bond energy that depends on the distance between the hydrophobic residues, $|\mathbf{d}_m|$. This distance can be defined with respect to the CA atom of the residue as we have done, or with respect to other atoms in the residue. This choice does not influence the final results, as long as the most favorable distance, D_0 is defined properly. The second and third terms constrain

the relative angle of the hydrophobic bond with respect the CC helices. We found this term is necessary to reproduce the correct force response. Without this term, the helices will tend to twist and slide with respect to each other when forces are applied. This is not seen in molecular dynamics simulations. Finally, the last term represents the hard-core repulsion between the helices. This term prevents the helices from physically penetrating each other.

When forces are applied to the CC e.g., at one end of the dimer, the conformational energy becomes

$$E = E - \mathbf{F} \cdot \left[\frac{\mathbf{r}(l) + \mathbf{r}'(l)}{2} \right] \tag{2.15}$$

where E is the same energy as Eq. (2.11). Eq. (2.15) implies that the force is applied at the mid-point between two helices, or the force is shared equally. The bending displacement $\mathbf{u}$ is therefore the difference in $(\mathbf{r}(l) + \mathbf{r}'(l))/2$ before and after the application of force. There are other situations where the force is only applied to one helix which can be similarly modeled.

2.2.3 Computation of Mechanical Equilibrium Configurations

Formally, in the presence of an external force, the equilibrium configuration of the CC can be computed by force and torque balance, which is equivalent to finding the minimum energy configuration of Eq. (2.15). The variables are the centerline

curves $(\mathbf{r}(s), \mathbf{r}'(s'))$ and the generalized torsions $(\omega_i(s), \omega_i'(s'))$. The minimum energy configurations are solutions of equations

$$\begin{aligned} \frac{\delta E}{\delta \mathbf{r}(s)} &= 0, \qquad \frac{\delta E}{\delta \mathbf{r}(s)} = 0 \\ \frac{\delta E}{\delta \omega_i(s)} &= 0, \qquad \frac{\delta E}{\delta \omega_i'(s')} = 0 \end{aligned} \tag{2.16}$$

In practice, the calculations are carried out by discretizing (s, s') into points $(s_k, s'_{k'})$ with $\Delta s = s_k - s_{k-1} = h_0 = 0.15$nm. The solutions of Eq. (2.16) is a set of vectors with components labeled by k or k'. The solutions are obtained using conjugate gradient search method. Gradients of the energy are computed numerically using 4th order finite difference. Multiple initial starting configurations are chosen to test the validity of the solutions.

2.2.4 Molecular Dynamics Simulations of Coiled Coil Under Force

We use the CC dimer domain of cortexillin I (PDBID:1D7M) for our MD studies. This is a relatively stiff CC with $P = 12$nm. By deleting residues starting from the C-termini, the length of the CC is modified such that we obtain a 12.6nm (13-Heptad) and a 8.4 nm (9-heptad) CC. In VMD [42] the structures are submersed in TIP3 water and the overall electrical charge is neutralized with Cl^- and Na^+ ions. The molecular dynamics simulations are performed using NAMD [43] with CHARMM27 [44] force field parameters. Particle Mesh-Ewald (PME) [45] is used for

electrostatics calculations. NPT ensemble and periodic boundary conditions with a rectangular box are applied. For the 9-heptad, system size is 4.5x12x4.5 nm and there are 20,000 atoms. For the 13-heptad, the system size is 4.5x16x4.5 nm and there are 27,000 atoms. The temperature (310 K) and pressure (1 atm) in the simulations are kept constant using Langevin dynamics. Initial energy minimization is done using conjugate gradient method. Equilibration is done for 60 ps by heating up the system from 0K to 310 K, and followed by 20 ns production (bending/twisting) runs. During the production runs, in order to emulate the clamped boundary condition on one end, positions of the first eight N-termini C_α atoms on both chains are fixed. These are GLU243-MET244-ALA245-ASN246-ARG247-LEU248-ALA249-GLY250 on A and B chains. The time step for the simulations is 2 fs. The trajectories are sampled at 10-ps intervals. We use MATLAB [46] to analyze the MD trajectories. The simulations are carried out in a Linux-based cluster with 8 nodes.

The bending responses of CCs to three different constant forces (7, 11 and 15 pN) are studied using MD simulations. The bending forces are applied at the instantaneous cartesian coordinates of the C-termini residue C_α atoms on both chains, i.e. residues GLU305-AB for the short CC and residues ALA333-AB for the longer. The force magnitude on the two atoms is half the total bending force magnitude. The forces are defined orthogonal to the plane spanned by two vectors: the initial centerline vector of the CCs and the vector defined by the difference between the initial positions of the C-termini C_α atoms of chains A and B. The instantaneous bending

displacement is calculated as the tip-to-tip distance between the bent(instantaneous) structure and the initial structure. Statistics are collected on the fluctuating structures for 15 ns, discarding the initial 5 ns.

For the CC twist calculations, we do not apply any torque to the structures. Instead, we gather statistics on the twist angle ϕ of Eq. 3. In order to calculate the angle ϕ, we first define triads along the centerline of the CC with a similar method as shown in Ref. [41]. Then, from the relative rotation of these local frames, the probability distributions of ϕ along the centerline are histogrammed for 15 ns. By fitting the probability distributions of ϕ, we find the twist persistence length, Λ_t, as a function of the CC length.

2.3 Results

2.3.1 Coiled Coil Pitch

The pitch of the CC dimer is directly measurable from X-ray structures. The mechanical model presented in this work can compute the pitch by finding the mechanical equilibrium configuration without external forces. We define the pitch based on the twist and bending of α-helix local frames (Fig. 2.1C) in the mechanical equilibrium configuration. Using Eq. (2.1), which gives generalized torsions on these local

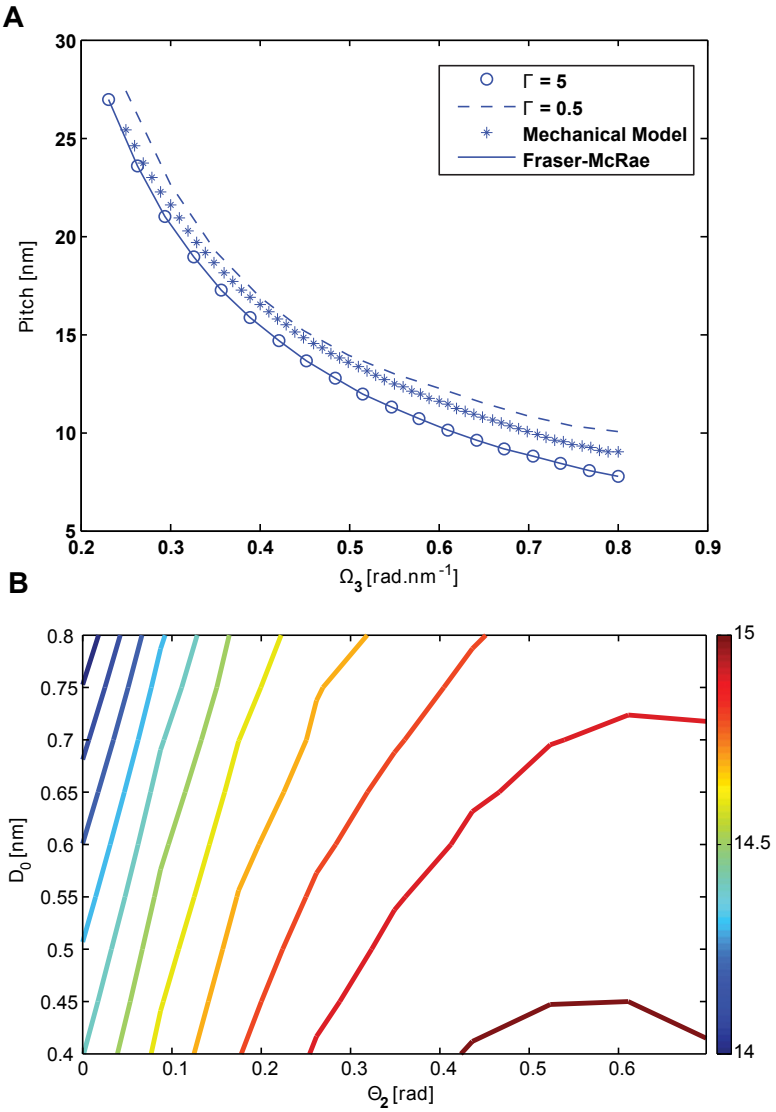

Figure 2.2: Pitch of the coiled coil. (A) Pitch is plotted as a function of the intrinsic twist of the hydrophobic residues in the α-helices, Ω_3. Wolgemuth and Sun's [16] prediction with $\Gamma = l_t/l_p$=5 (circles), $\Gamma = 0.5$ (dashed line) is shown. The solid line shows the solution to the Fraser and MacRae equation [11]. The crosses are the mechanical model predictions for a 13-heptad repeat coiled coil. (B) The dependency of the coiled coil pitch on the geometric parameters D_0 and Θ_0. The pitch varies less than 10%, which suggests that mechanical constants k_1 and k_2 have a negligible effect on the geometrical properties of the coiled coil.

frames, the pitch P is:

$$P = \frac{2\pi w_3}{w_1^2 + w_2^2 + w_3^2} \tag{2.17}$$

In general, because of the discrete hydrophobic residues in our model, ω_i is a function of the arclength s. Here, we report the pitch value averaged over the length of the CC in Fig. 2.2.

The pitch strongly depends on the value of the helix intrinsic twist, Ω_3. For historical reasons and simplification purposes, the angle between hydrophobic residues α is taken to be $\alpha = 2\pi/3.6 = 100°$. In fact, as Chothia [47] and Phillips pointed out [30] there are an average of 3.64 residues in every α-helix turn, thus yielding $\alpha = 98.9°$. This small difference may seem insignificant, but it has a profound influence on the CC pitch because Ω_3 changes from 0.33 rad/nm to 0.46 rad/nm. Fig. 2.2A shows the predicted pitch as a function of Ω_3. We see that the pitch changes by 50% as α changes by 2°! For most α-helices, Ω_3 ranges from -0.2 to -0.9 [47].

In our CC model, the hydrophobic bond energy is defined by additional parameters: k_1 and k_2 are the bond distance stiffness and bond angle stiffness, respectively. D_0 is the equilibrium hydrophobic bond length and $\Theta_{1,2}$ are the equilibrium hydrophobic bond angles (see *Models section*). We find that choices of stiffness parameters, in general, have a small effect on the CC pitch. However, geometric parameters D_0 and Θ_2 have a more pronounced effect (Fig. 2.2B). As the hydrophobic bond length and contact angles are varied, the pitch varies by roughly 10%. Θ_2 also has a more pronounced effect than Θ_1. These parameters, along with sequence inhomogeneity,

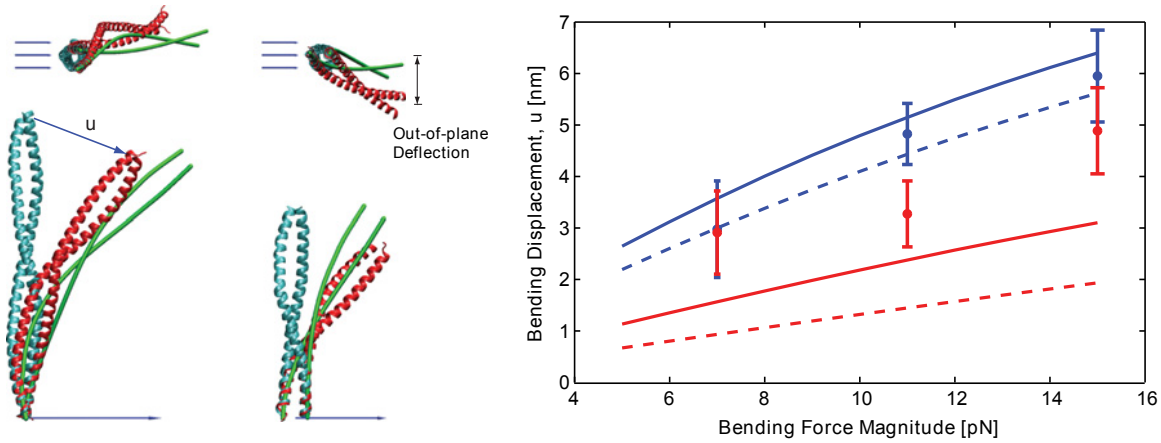

Figure 2.3: Bending response of the CC model compared to molecular dynamics simulations. The bottom end of the CC is clamped (both position and orientation of the material frame are fixed). The applied force is directed to the right (vectors). The average MD structures before (cyan) and after (red) the application of the bending force is shown, along with the coarse-grained mechanical model (green lines). Views from the side and top are shown. The right plot shows the magnitude of the bending displacement, $|\mathbf{u}|$, versus the magnitude of the applied force for the 8.4nm (red) and 12.6nm (blue) CC. The lines represent the predictions of the mechanical models: current model (solid lines) and Wolgemuth and Sun's [16] prediction with $\Gamma = 0.5$ (dashed lines). The MD results (symbols) with error bars are compared to model predictions (lines). Both MD and the CC model show a significant bending response perpendicular to the applied force direction (out-of-plane deflection), although our model shows a smaller out-of-plane deflection (0.5 nm) when compared to the MD result (2.0 nm) at 15pN bending force.

will contribute to the diversity of CC pitches observed in protein structures.

2.3.2 Coiled coil Bending and Buckling

CCs often serve as mechanical linkages between protein domains. It is therefore important to address the response of the CC to external force. Here we examine the bending property of the CC and ask whether it can be effectively modeled as a thin rod. Using our coarse-grained mechanical model and Eq. 2.15, we compute the response of the CC under forces ranging from 5 to 15 pN (Fig. 2.3). The computed bending displacement, $\mathbf{u}$, is compared to molecular dynamics simulations of real protein structures in explicit solvent under a constant force. Fig. 2.3 shows the molecular structures of the CC under force and the observed deflections. MD simulations are performed on two different CCs (8.4 and 12.6 nm in length) and 3 different forces: 7, 11 and 15 pN. After equilibrating, we collect statistics on the fluctuating structure for 15ns. The shown structure is the average equilibrium structure of the CC. Superimposed on the MD results are the results our coarse-grained mechanical model results. The model has no free parameters except for stiffnesses k_1, k_2 and k_3. The best fit results are shown in Fig. 2.3. The model suggested by Wolgemuth and Sun [16] constrains the distance between helices and does not allow the helices to slide with respect to each other, which can be thought of as $k_1 = k_2 = \infty$ in our present model. We see that both models compare well with MD results, although WS is significantly worse for short CCs. By allowing finite stiffness, our current model is better matched

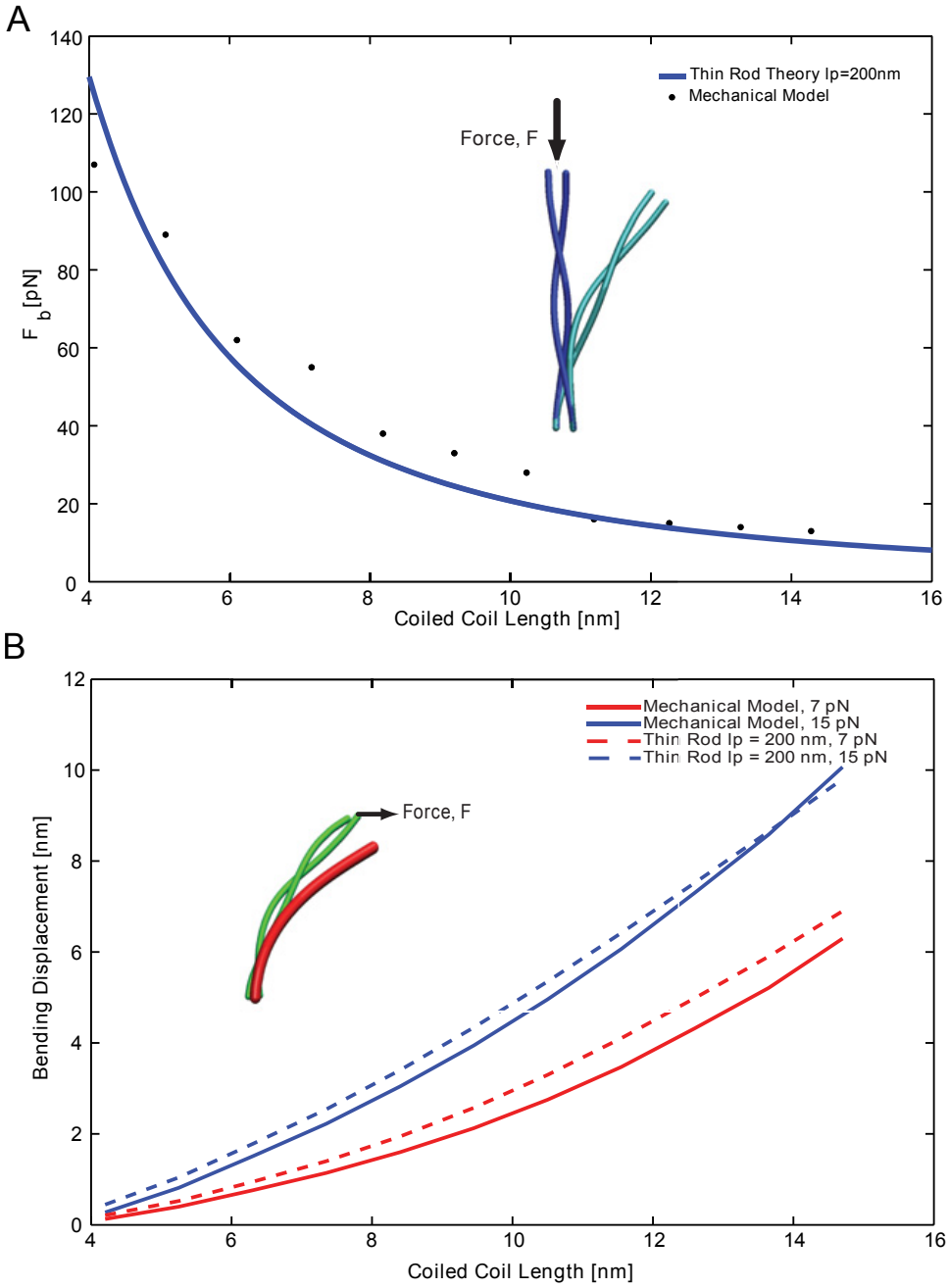

Figure 2.4: Bending response of the coiled coil compared to a slender rod. (A) A vertical force is applied to buckle the coiled coil structure. Our model shows that the critical buckling force as a function of the CC length (points) is well described by the buckling of a slender rod (solid line) in Eq. (2.18). The fitted CC persistence length, l_p =200nm. However, the bending response of the coiled coil is not completely described by a slender rod. (B) shows the comparison between our model with the slender rod bending response with rod l_p =200nm.

with the MD results. The MD result also shows additional complex behavior that is not captured by our model. Perhaps additional long range interactions suggested by Lakkaraju and Hwang [35] can improve the model predictions.

Both the MD and the mechanical model show responses to the applied force that are not replicated by a slender rod. For example, when a slender rod is subjected to a force at one end with the other end held fixed, the deformation of the rod is confined within the plane spanned by the force vector and the opposite end. For the CC, we observe a substantial deflection in the out of plane direction (Fig. 2.3). This is because the α-helices are not confined to the bending plane, there is a significant component of the torque in the direction perpendicular to the deflection plane. The complete problem requires considering the bending response of helical rods, which is beyond the scope of the work here. Nevertheless, MD and our model show similar qualitative out-of-plane movement.

By examining the bending response of the CC, we also can estimate the effective bending persistence length (bending modulus) of the CC. There are several ways to obtain this estimate. Fig. 2.4A shows the Euler buckling response of the CC. The position and orientation of the CC is fixed at one end. The other end is subjected to a vertical downward force. The critical buckling force is compared with the rod theory prediction:

$$F_b = \frac{\pi^2 l_p k_{\mathrm{B}} T}{4L^2} \tag{2.18}$$

where L is the length of the CC and $k_{\mathrm{B}}T = 4.2\mathrm{pNnm}$. The coarse-grained mechanical

model behaves quite similar to the rod theory. The best fit that gives the effective bending persistence length of the CC is l_p =200nm, although a range of persistence length from 160-200nm can all explain the observed buckling force. However, when a horizontal force is applied that bends the CC, the response is again somewhat different from the slender rod model with l_p = 200nm (Fig. 2.4B). Aside from the observed out-of-plane bending, the net displacement as a function of the CC length is also consistently less than predictions of the rod model with $l_p = 200$nm. Suggesting that the CC may be slightly stiffer than the effective rod prediction. The length dependence of the bending displacement also behaves differently than a standard rod. Therefore, describing the CC as a rod with a single bending constant is problematic. Bathe et al. [48] predicted that the bending response of parallel bundles will have a component that depend on the stretching of the transverse bonds. The overall bending constant of the bundle is also length dependent (mode-dependent bending). This is consistent with our model which shows a length dependent bending modulus and shows that CCs cannot be described as simple rods with a fixed mechanical bending modulus. This result has important implications in mechanics of motor proteins where force transmission between motor domains are carried out by CCs [49].

2.3.3 Coiled Coil Twist

Twisting of CCs is a common deformation encountered in proteins. The connection between cargos and molecular motors are often made of CCs, and the processive

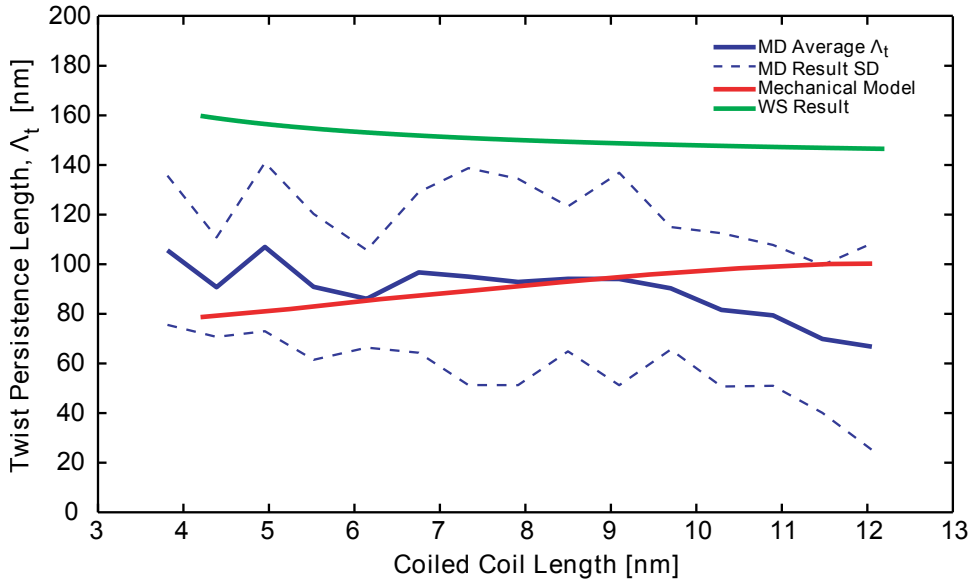

Figure 2.5: Twist persistence length, Λ_t, of the coiled coil. From MD simulations, the twist persistence length (blue line) can be estimated from the angular fluctuations of the coiled coil twist, in a manner similar to Ref. [41]. The model prediction (red line) is obtained from applying a known torque to the CC structure and compute the twist response. Also shown is Wolgemuth and Sun's [16] prediction with $\Gamma = 0.5$ (green line). Results show that the twist persistence length of the coiled coil is around 100nm, although there is some length dependence.

(walking) motion of the motor introduces torsion into the CC domain. To obtain an estimate of the twist modulus of the CC, we examined MD simulation results and our coarse-grained model predictions. For a straight rod only undergoing twist deformations, the conformational energy is

$$E = \frac{1}{2}\int_0^L l_t k_{\mathrm{B}} T(\omega_3 - \Omega_3)^2 ds = \frac{1}{2}\frac{\Lambda_t}{L} k_{\mathrm{B}} T \phi^2 \tag{2.19}$$

where L is the rod length, Λ_t is the twist persistence length and ϕ is the twist angle at the end of the rod. In MD, we have examined the conformational fluctuation of the CC and obtained probability distribution of the twist angles. From the probability distributions, which are roughly Gaussian functions of ϕ, we obtained the twist persistence length, Λ_t, as a function of the CC length (Fig. 2.5). The simulation result is compared to our coarse-grained model, where we have examined the response of the CC to an applied torque. The comparison shows that CC has a twist persistence length of $\sim$100nm. However, the twist persistence length depends on the length of the CC, which implies nonlinear behavior. Our model agrees with the MD results for CC lengths around 10-12nm. For shorter lengths, the applied torque generates twist by twisting the individual α-helices. For longer lengths, the applied torque bends the α-helices and reduces the CC pitch. The prediction of WS (see Appendix of [50]) suggests a slightly higher twist persistence length, presumably because the angular springs characterizing the hydrophobic bond are flexible in reality. WS assumes a completely rigid interaction in the hydrophobic bond.

2.3.4 Conformational Amplification

So far, we have focused on the overall mechanical behavior of the CC. We have compared the CC response to rod-like objects. However, the CC has more complicated mechanical responses that are biologically important. For example, the microtubule binding domain of dynein appears to undergo a deformation where one helix is shifted with respect to the other [38, 39]. Small molecules can also bind the CC and induce a small local conformational change. The Tar receptor of *E. coli* binds an aspartate molecule at one end of the CC. Upon binding, this molecule shifts one helix with respect to the other, and introduces a piston motion along the centerline of the CC of about 1.6Å [51]. We find that our model predicts a significant amplification of this type of conformational change, defined as m_2/m_1 where m_1 is the magnitude of the pistoning displacement and m_2 is the bending displacement at the distal end (Fig. 2.6). For example, for a 40nm long CC, $m_1 = 1.6$Å translates to a bending movement of $m_2 = 5$nm, a 30 fold amplification. Note that the free energy needed to introduce the small piston displacement is quite small and can derive from the binding free energy of the small ligands (Fig. 2.6). The amount of amplification depends on the length of the CC. Along the same lines, if a small twist at the end of one of the helices is introduced, a bending motion also can occur in the distal end. A twist of 90 degrees in one of the helices can translate into a small bending movement at the distal end, although the degree of amplification is significantly less.

Fig. 2.6B shows the strains in the hydrophobic bonds in a 40nm CC with an

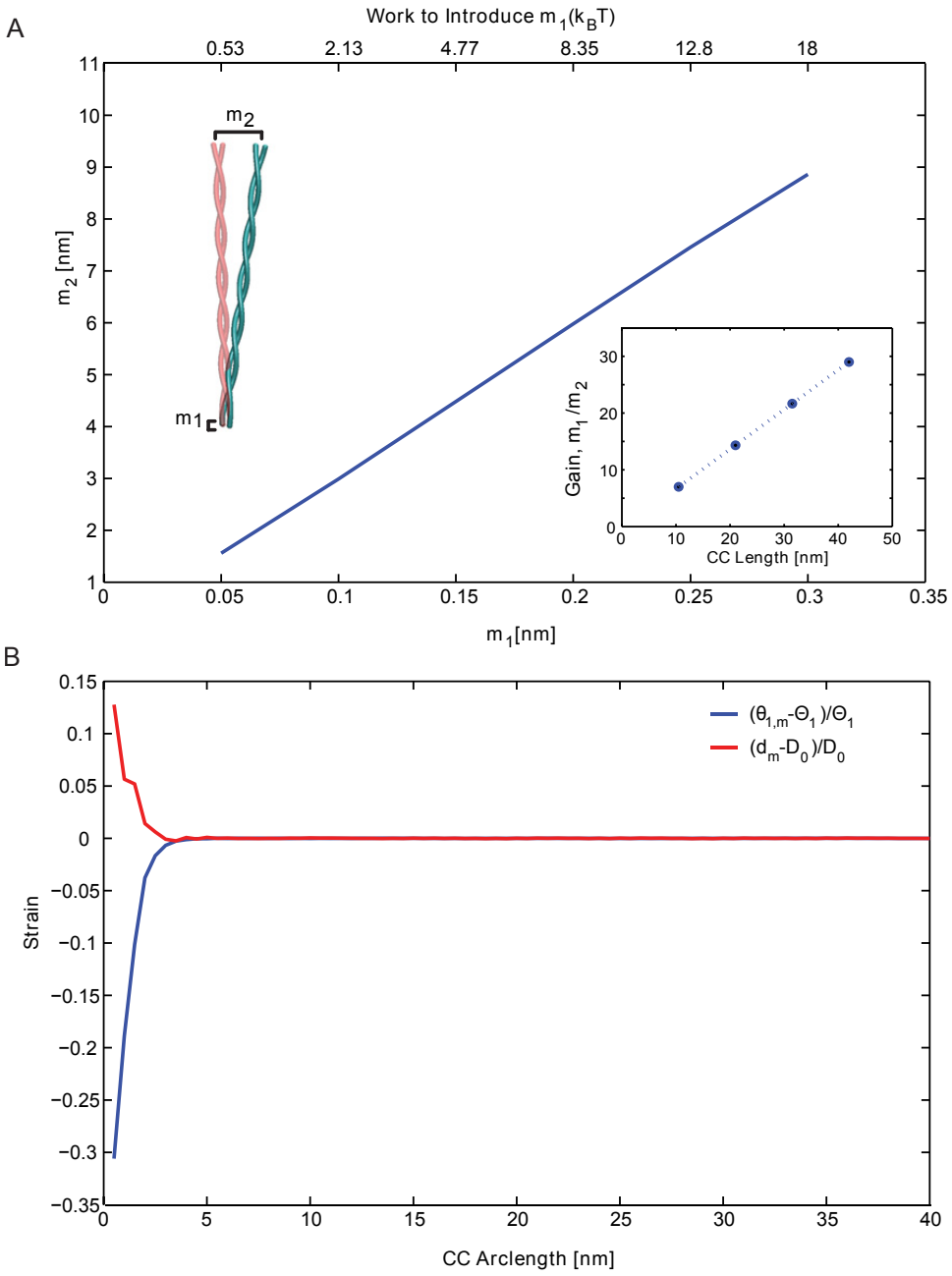

Figure 2.6: Conformational amplification in the coiled coil. (A) At one end of the CC, we introduce a small conformational change in one of the α-helices while keeping the other helix fixed. A small piston displacement or vertical movement of size m_1 translates to a bending motion of size m_2 at the distal end. The top axis shows the amount of mechanical work needed to introduce the m_1 movement. The inset shows the conformational gain as a function of CC length. (B) The strain in $\theta_{1,m}$ and d_m as a function of the CC arclength, s. A piston movement of 0.3nm is introduced to a 40nm CC at $s = 0$. Most of the strain is concentrated near the position of movement.

initial piston movement of 0.3nm. Most of the significant strains occur within the first 5nm of the CC. There is also significant bending strains in the α-helices. In an experiment such as in Ref. [39] where the α-helices are artificially tied together using disulfide bonds, the overall bending of the CC can be prevented.

This suggests that the elasticity of protein structures can transmit and amplify conformational signals over long distances, and may explain the action of small ligands binding to CC structures. In the Tsr receptor, the distal end of the receptor contacts other signaling proteins and neighboring receptors, leading to cooperativity between receptors. Our model suggests that the cooperativity arises from intrinsic mechanical properties of α-helical bundles. This mechanism is in contrast to the "wedge" mechanism of Yu and Koshland [52], which invokes a series of bond re-arrangement to explain the propagation of small conformational changes. Since proteins are mechanical structures, a more plausible mechanism involves large scale flexible movements based on geometrical arrangement of protein components.

2.4 Discussion

In this work, we explored the conformational properties of the CC in response to applied forces and torques, and developed a coarse-grained mechanical model to describe the conformational dynamics. The model treats the CC motif as two elastic α-helices bonded together by a regular pattern of hydrophobic bonds. The model is

able to quickly compute the conformational response of long CCs without resorting to costly atomistic simulations. The model is also compared to MD simulations for short CCs. Our model is able to reproduce most of the bending and twist response observed in MD simulations, suggesting that the model is a reasonable representation of the actual protein structure. Of course, there are other ways of parameterizing the model and the hydrophobic bonds, but it is clear that the model must consider angular constraints provided by the hydrophobic interactions. Our model can also be made more quantitative by considering the sequence dependence of the hydrophobic interaction, which can be added by introducing sequence-dependence in parameters listed in Table 2.1. Additional factors such as possible long range interactions are not considered here, but could be important for longer CCs.

While the elastic properties of the α-helix is reasonably simple, we find that the CC shows more complex mechanical properties. For example, from examining the buckling properties of CCs, it is possible to estimate the CC bending persistence length of 200nm, approximately two times the persistence length of the α-helix. Experimental measurements of CC persistence length exist in literature [53–55]. However, different measurement techniques seem to yield significantly different results. Part of the reason could be the length dependence of the CC mechanical response and the way external forces are applied in the measurements. We also find that CCs are more complex, and a simple rod model does not explain all the bending responses. For instance, the bending displacement has a component that is out of the plane of the bending

force. The bending persistence length also appears to be slightly length dependent. The twist persistence length shows a similar complexity and length dependence. CCs are often domains in motor proteins that connects the motor to the cargo. In single molecule experiments, the motion of the cargo is tracked and observed. Our study shows that the cargo motion is not a direct reflection of the motion of the motor because of the complex response of the CC domain.

For real proteins, if sufficient forces are applied the hydrophobic bonds will eventually break, leading to possible unfolding of the structure. Indeed, studies suggest that the hydrophobic bond energy is roughly $10k_{\mathrm{B}}T$. In our model, the spring-like interaction potential does not allow the bonds to break. To introduce structures that can fail, it is possible to define the interaction potential by introducing a cutoff. If the total energy of the bond, ΔE, exceeds the cutoff, the bond fails. With this, we find that CCs can with stand significant forces before failing, although the direction of the applied force and the length of the CC are important. For example, for perpendicularly applied bending forces such as in Fig. 2.3, the 13nm structure can withstand 100pN before breaking of the hydrophobic bonds are observed. In biologically relevant situations, molecules rarely experiences forces of such magnitude. For example, molecular motors often exert forces that are less than 10pN. Therefore, we expect that CCs function mostly as a folded and intact structure during common deformations.

CC domains in proteins are often involved in mechanotransduction and chemical signaling. Our model suggests that these functions can be explained within one unified

picture. The CC structure responds to externally applied forces and changes conformation over long distances. We also discover that the CC structure responds to local and small perturbations and amplifies them over long distances. The amplification depends on the length of the CC, and may explain why the bacterial chemoreceptor is nearly 40nm in length. The amplification also suggests that cooperative properties of receptor arrays may be mechanical in origin, and mechanical properties of proteins is an important aspect for understanding protein function in general.

Chapter 3

A Mechanochemical Model of Actin Filaments

In eukaryotic cells, actin filaments are involved in important processes such as motility, division, cell shape regulation, contractility and mechanosensation. Actin filaments are polymerized chains of monomers, which themselves undergo a range of chemical events such as ATP hydrolysis, polymerization and depolymerization. When forces are applied to F-actin, in addition to filament mechanical deformations, the applied force must also influence chemical events in the filament. We develop an intermediate-scale model of actin filaments that combines actin chemistry with filament-level deformations. The model is able to compute mechanical responses of F-actin during bending and stretching. The model also describes the interplay between ATP hydrolysis and filament deformations, including possible force-induced chemical

state changes of actin monomers in the filament. The model can also be used to model the action of several actin-associated proteins, and for large-scale simulation of F-actin networks. All together, our model shows that mechanics and chemistry must be considered together to understand cytoskeletal dynamics in living cells.

3.1 Introduction

Actin filaments play central roles in important cellular processes such as motility, division, morphogenesis, cell shape regulation and mechanosensation. In cells, actin monomers polymerize into dynamic filaments that form an entangled network. Filaments in the network are constantly undergoing changes such as polymerization and depolymerization, branching and severing/fragmentation. This dynamic morphological change enables the network to remodel itself in response to external stimuli. Actin polymerization and depolymerization have been studied in vitro and in vivo [15, 56, 57]. The mechanical properties of actin networks also have been examined in a range of experiments, from single filaments [58–60] to networks with actin associated proteins [61]. These experiments demonstrate that actin possesses unique mechanical and chemical properties, yet many of these observations have not been explained theoretically. In particular, there does not exist a unified model where the mechanics and chemistry of actin are considered together on an equal footing. Here, we develop such a mechanochemical model, and demonstrate that forces can have

a strong influence on actin chemistry. This mechanochemical coupling may explain some of actin's unique properties in the cell. The model is also applied to examine the role of several actin associated proteins. The model represents an intermediate scale description of actin filaments, which provides a crucial link from the molecular scale to the cytoplasmic cellular scale.

There have been many important studies on the unique roles of actin in the cell. For instance, a molecular mechanism of actin-driven cell motility, together with the action of actin associated proteins have been proposed [56, 62, 63]. Actin filaments polymerize at the cellular leading edge, and extend the membrane forward. Arp2/3 promotes branching of new filaments from existing filaments. Slightly behind the leading edge, ADF/cofilin promotes severing of existing actin filaments [56, 64, 65] while transmembrane integrin adhesions form between filaments and the extracellular substrate to anchor the leading edge. These processes are known to control the filament length distribution and dynamics of filament turnover [66, 67]. Dynamics of actin filaments is also known to be involved in other important cellular functions such as endocytosis [68, 69] and cytokinesis [69, 70]. A common feature during these processes is that actin filaments are under the action of mechanical forces, either from the cell membrane or molecular motors. Actin network remodeling, together with the activity of non-muscle myosin II and adhesion molecules, also play a crucial role in cellular mechanosensation [71–73]. A recent modeling study has shown how actin-myosin bundles (stress fibers) can form in response to cell substrate mechanical

stiffness [73]; although, it is also pointed out that actin filaments alone can have mechanosensing properties [74]. These properties mostly arise from structural changes in the actin filament under external forces. Therefore, an improved understanding of actin mechanical response and how forces can regulate actin chemistry are important for elucidating the mechanisms of actin function in the cell.

Actin filament is a staggered double helix formed by nucleation and directional polymerization of G-actin monomers [57]. The monomers that polymerize on the same helix are connected via longitudinal bonds (non-covalent interaction) while the monomers on two opposite helices interact through diagonal bonds. The intrinsic bond energy of a longitudinal bond was shown to be three times larger than a diagonal bond [75]. The filament subunits can be found in three bound nucleotide states, ATP, ADP and the reaction intermediate ADP.Pi. The bonds between subunits with ATP are lower in free energy [76]. Recent studies [77–79] have proposed full atomistic models of actin filaments by fitting the known atomic structures of G-actin monomers into low resolution electron microscopy images. However, there is accumulating evidence that F-actin is an inherently polymorphic filament [74,80–82]. The structural polymorphism also potentially affects the mechanical properties of single filaments.

Mechanical properties of actin filaments and networks have been studied extensively [21,61]. In particular, computational [83,84] and experimental [58–60,85] studies on the persistence length of the actin filament have been performed. Although the

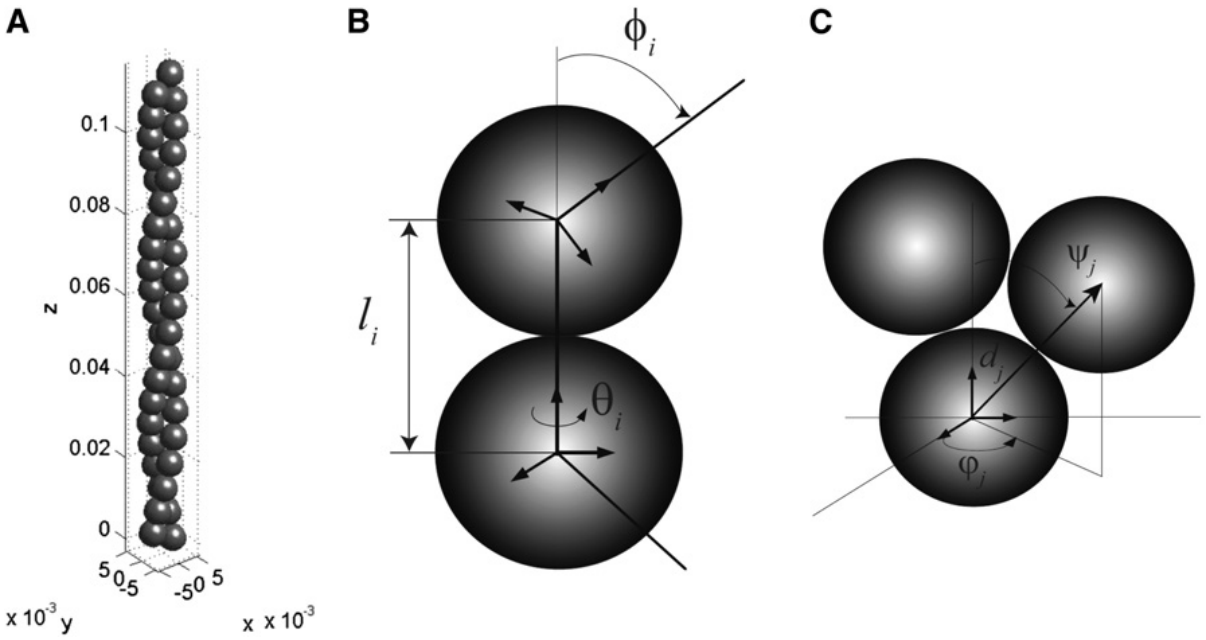

Figure 3.1: A coarse-grained model of an actin filament. (A) The model represents the filament as two helical chains of monomers staggered with respect to each other. The configuration of the filament is described by bond distances, bond angles and local material frames attached to each monomer (see Methods). (B) The interaction between intra-strand monomers is defined by bond distance l, relative twist angle θ, and relative bending angle ϕ. (C) The interaction between inter-strand monomers is defined by bond distance d, relative twist angle φ, and relative bending angle ψ. For detailed definitions, see Methods.

average persistence length with all subunits in the ATP state (F-ATP) is about 17μm, the data shows a large variation ranging from several to a few tens of microns [59]. One of the factors that can affect bending stiffness is the nucleotide state of the subunits, i.e., ATP or ADP [58, 86]. From computational studies, F-ATP was found to be twice as stiff as F-ADP, and this is attributed to a structural change of DNase I-binding loop in subdomain 2 [87,88]. The identity of the bound nucleotide is not the only factor that could affect filament stiffness. Due to the helical structure of F-actin, mechanical coupling of bending and twist was shown to be important, especially for short filaments [89]. In addition, factors such as ions, pH, drugs and other proteins can change filament behavior [58]. Actin interacts with more than a hundred different actin binding proteins (ABPs) and these interactions alter the intrinsic mechanical properties of actin filaments and networks. Among these, Arp2/3 and Cofilin are two well studied examples [90, 91]. Cofilin cooperatively severs actin filaments by increasing the intrinsic longitudinal bond length and decreasing the pitch of the staggered helical actin structure while the actin filament length stays the same [74,92,93]. Also, Cofilin-decorated actin filaments are experimentally found to be 4 times softer than standard F-Actin [93]. It was shown that the most probable location of severing on the filament is at the boundaries between cofilin decorated and bare actin region [94, 95]. On the other hand, Arp2/3 promotes actin filament branching by nucleating new filaments at an angle 70° with respect to the mother filament [96]. A recent experimental study demonstrated that Arp2/3 binds preferentially to the

convex side of a bent filament [97]. This has clear implications on filament branching especially at the cellular cortex region where actin is under large bending forces.

Chemical and mechanical properties of actin have been two separate directions for modeling studies. Extensive experimental studies [15] have provided rich information on chemical kinetics of actin and its binding partners, and paved the way for elaborate simulations [95, 98–102]. Mechanical behaviors of actin monomers [87] and filament models [84, 93] have been studied with detailed molecular dynamics (MD) simulations. However, MD currently cannot access filament-scale biologically relevant phenomena. Therefore, coarse-grained (CG) models have been proposed at the cost of lost atomistic detail [83, 103–105]. Elastic rod theory has been also previously used to study F-actin buckling and force production [106] and filament severing by cofilin [107]. These studies provide important insights into global F-actin behavior. How the global behavior is affected by the interaction between helical strands and nonlinearities such as local perturbations on elasticity, single actin subunit kinematics and cooperativity yet remains as an active area of research. To fully understand the role of actin in the cell however, it is important to develop models that can examine the interplay between mechanics and chemistry [108]. Currently, a detailed mechanochemical model of actin filaments does not exist. In this work, we build a simple mechanical model of the actin filament that can simultaneously compute filament deformations as well as internal chemical kinetics. We parameterize the model using available experimental and computational data, and use the model to address

chemical state changes when the filaments are under external forces. The model combines stochastic chemical dynamics with mechanical deformations. We outline the basic framework of the model in the next section. After the discussion of the obtained results, we address how the model can be improved for larger scale simulations and predictions.

3.2 Methods

The undeformed actin filament is a straight double helical structure shown in Fig.3.1A. The monomer is roughly 6 nm in diameter and the pitch of the double helix is 72 nm [109]. Within the double helix, monomers bind to each other through non-covalent interactions, forming longitudinal bonds between monomers in each helical strand and diagonal bonds between adjacent monomers in opposite helical strands [75]. The monomer is also structurally asymmetric. Therefore, the configuration of the monomer is described by the position of its center of mass as well as a coordinate frame that describes its orientation in space. We describe the interaction between actin monomers using a set of linear and angular bonds. The bond variables are described in Fig.3.1.

In addition to the mechanical model, monomers in F-actin can have either ATP, ADP.Pi or ADP in the nucleotide pocket. The mechanical properties of the monomers depend on its chemical state. Therefore, our mechanical bond model depend on the

Table 3.1: Bond stiffness parameters, bond free energies and intrinsic geometric parameters for our model.

	ATP–ATP	ADP–ADP
k_ℓ [pN/μm]	4.8×10^6	4.29×10^6
k_θ [pN·μm]	0.27	0.12
k_ϕ [pN·μm]	0.33	0.17
k_d [pN/μm]	9.99×10^3	9.71×10^3
k_φ [pN·μm]	5.4	5.1
k_ψ [pN·μm]	1.2	0.5
ΔG^{long} [$k_\text{B}T$]	-20.07	-18.07
ΔG^{diag} [$k_\text{B}T$]	-8.08	-6.08
ℓ_0 [nm]	6.00	6.00
θ [°]	28.55	28.55
ϕ [°]	-6.43	-6.43
d_0 [nm]	6.00	6.00
φ_0 [°]	104.27	104.27
ψ_0 [°]	60.00	60.00

chemical states of the monomers. In this work, we specify the parameters for ATP-ATP and ADP-ADP bonds (Table 3.1).

Finally, when actin filaments are under external force, the applied force will influence chemical transitions in the monomers. We investigate the influence of this mechanochemical coupling by developing a simple model for the transition rate between chemical states. We use this model and the Gillespie simulation algorithm to investigate how F-actin deforms under forces.

3.2.1 The Mechanochemical Model

Binding interaction between actin monomers can be thought of as a deformation free energy as a function of the vector connecting the centers of mass and relative orientations of the coordinate frames. Such a model would involve 6 kinematic variables, 3 for translation and 3 for rotation, but would have a large number of parameters, most of which are currently unknown. For describing bonds between actin monomers, however, motions that give rise to sliding of one monomer on the surface of the other, and rolling of the monomers with centers of mass fixed are likely not allowed (note that in both cases, the bond length remains the same). These motions should not be introduced because they lead to dislodging of the actin-actin binding interface. This eliminates two translational variables and a rotational variable. Therefore, the simplest model involves three variables, describing the distance between the centers of mass and two angular variables related to the relative orientations of the coordi-

nate frames (Fig.3.1). Each longitudinal bond is parameterized by the bond length ℓ, torsion angle θ, and bond angle ϕ. Likewise each diagonal bond vector $\mathbf{d}$ is described with bond length d and two angular variables φ and ψ. The definitions of variables for the longitudinal and diagonal bonds are shown in Fig.3.1B and C. These kinematic variables can all be written as functions of monomer positions $\mathbf{p}_i$.

Binding free energies for longitudinal and diagonal bonds have been reported in the literature [75]. The mechanical free energy as a function of the kinematic variables, however, is likely complicated. Here we consider small deformations and expand the free energy to quadratic order around the equilibrium geometry of the filament. Specifically, we consider an expansion of the free energy E around the reference configuration: $E = E_0 + \frac{1}{2}(\mathbf{v}-\mathbf{v}_0)^T \left.\frac{\partial^2 E}{\partial \mathbf{v}^2}\right|_{\mathbf{v}_0} (\mathbf{v}-\mathbf{v}_0)$, where $\mathbf{v}$ is the vector of kinematic variables $(\ell, \theta, \phi, d, \varphi, \psi)$, and $\left.\frac{\partial E}{\partial \mathbf{v}}\right|_{\mathbf{v}_0} = \mathbf{0}$. E_0 is a constant that is the energy of the reference configuration, and the second term is written as a sum of quadratic terms without bilinear coupling. In total, the free energy can be written as

$$\begin{aligned} E = &\sum_{n=1}^{2}\sum_{i=1}^{N_b}\left(\Delta G^{\text{long}} + U_i^{(n)}(\ell_i^{(n)},\, \theta_i^{(n)},\, \phi_i^{(n)})\right) \\ &+ \sum_{j=1}^{N_d}\left(\Delta G^{\text{diag}} + V^{(j)}(d_j,\, \varphi_j,\, \psi_j)\right) \end{aligned} \tag{3.1}$$

where

$$U_i^{(n)} = \frac{1}{2}k_\ell(\ell_i^{(n)} - \ell_0)^2 + \frac{1}{2}k_\theta(\theta_i^{(n)} - \theta_0)^2 + \frac{1}{2}k_\phi(\phi_i^{(n)} - \phi_0)^2 \tag{3.2}$$

with $n = 1$, 2 denoting the identity of the strand, and

$$V^{(j)} = \frac{1}{2}k_d(d_j - d_0)^2 + \frac{1}{2}k_\varphi(\varphi_j - \varphi_0)^2 + \frac{1}{2}k_\psi(\psi_j - \psi_0)^2. \tag{3.3}$$

Here, ΔG^{long} and ΔG^{diag} denote the bond free energies for the longitudinal and diagonal bond, respectively. N_b denotes the number of longitudinal bonds in each helix, which is also related to the number of monomers N_m in each helix as $N_b = N_m - 1$. N_d denotes the number of diagonal bonds and is given as $N_d = 2N_m - 1$. When external forces are applied, the filament will deform and change shape, the work done by the external force is included in the energy by adding the work term as

$$W = -\mathbf{f} \cdot \mathbf{p}_{2N_m} \tag{3.4}$$

where $\mathbf{p}_{2N_m}$ denotes the position of the monomer at the distal end where external force $\mathbf{f}$ is applied. The center of mass positions and the coordinate frames of the first monomers of each strand have been fixed. These frames are chosen such that the centerline of a relaxed filament lies along the z-axis. The direction of $\mathbf{f}$ is parallel to $\mathbf{z}$-axis for stretching and orthogonal to $\mathbf{z}$-axis for bending. The mechanical equilibrium shape of the filament is obtained by minimizing the total energy with respect to the positions and orientations of all monomers for the given boundary conditions. Therefore, for a purely mechanical treatment of F-actin, the equilibrium conformation depends only on the equilibrium bond variables but not the intrinsic bond energies. One can also examine thermal fluctuations around the mechanical equilibrium configuration using this model.

An important feature of actin is that the monomer can adopt different chemical states. Thus, all of the model parameters in Eq. 3.1 are potentially functions of the chemical state of the monomer (Table 3.1). In principle the monomers can have ATP,

ADP.Pi or ADP in the nucleotide pocket. Transitions between these chemical states are described by rate constants. The rate of irreversible hydrolysis of ATP to ADP.Pi within the subunits is on the same order of F-actin polymerization and the conversion from ADP.Pi to ADP state is 100 times slower than ATP-ADP.Pi hydrolysis [15]. As a result, in a filament, the number of subunits with ADP.Pi and ADP is significantly higher than that of ATP subunits. Here we consider a simplified set of chemical states by representing ADP.Pi state as an ATP state and assume that these two states have similar bond energetics and mechanical properties.

The bond free energies, ΔG^{long} and ΔG^{diag}, are dependent on the chemical state of monomers involved in each bond and ΔG^{long} is significantly lower than ΔG^{diag} [79]. For example, when both monomers are in ADP states, it is estimated that $\Delta G^{\text{long}} = -18.07\, k_{\text{B}}T$ and $\Delta G^{\text{diag}} = -6.08\, k_{\text{B}}T$ [75]. Here k_{B} and T denotes the Boltzmann constant and absolute temperature, respectively. ATP hydrolysis in actin filaments has been shown to be fast and irreversible, and ADP.Pi state is the intermediate and rate limiting state [15]. In physiological conditions, the actual free energy difference is small ($<0.5\ k_{\text{B}}T$), albeit a decreasing function of inorganic phosphate concentration in the medium. For illustrating mechanochemical effects, we use $2k_{\text{B}}T$ [76] as the free energy difference in this work, with the understanding that Pi concentration can influence this number. From this information, we can infer the intrinsic free energy for ATP-ATP and ATP-ADP bonds, which is listed in Table 3.1.

In addition to bond energies, bond stiffnesses $(k_\ell, k_\theta, k\phi)$ and (k_d, k_φ, k_ψ), as well as

equilibrium configurations $(\ell_0, \theta_0, \phi_0)$ and (d_0, φ_0, ψ_0) are all potentially functions of monomer chemical state. There is potentially a set of parameters for each ATP-ATP, ATP-ADP and ADP-ADP bond. From actin filament structural studies, there is no evidence of structural differences between ATP and ADP filaments. For example, if ℓ_0 is different in ATP vs. ADP monomers, the overall length of the filament would depend on the monomer chemical state. Therefore, we assume that the equilibrium configurations are independent of the bond type. However, mechanical properties of the filament does depend on the nucleotide states, and therefore there are potentially three sets of stiffnesses in our model. How we obtain the ATP-ATP and ADP-ADP stiffness parameters are discussed in the next section. We also assume that ATP-ADP stiffness parameters are the average of the ATP-ATP and ADP-ADP parameters.

Transitions between chemical states are usually described by chemical reaction rates. Because the configurations of the monomers can potentially change with the chemical state, the reaction rates are not constants but are reaction rate functions [110,111]. This framework has been used for muscle contraction [112], molecular motors [110, 113] and enzyme turnover [114] in general. Indeed, if the global conformation of actin is somehow fixed, hydrolysis would still proceed. Therefore, the total energy of the filament is actually a function of monomer positions, $\mathbf{p}_n$ and monomer chemical states

$$E \equiv E(\mathbf{p}_1, \ldots, \mathbf{p}_{2N_m}, s) \tag{3.5}$$

where s is an integer that labels the chemical state of the filament. If each monomer

can be in ATP or ADP states, then s ranges from 1 to 2^{2N_m}. If we are interested in rupture of actin filaments, the bonds between monomers can also break. This implies that the number of states is potentially $2^{2N_m} \times (2N_b + N_d)$ (see below). The transition rate functions satisfy detailed balance

$$\frac{k_{s\to s'}}{k_{s'\to s}} = \exp\left[-\beta(E(\mathbf{p}_1,\ldots,\mathbf{p}_{2N_m},s) - E(\mathbf{p}'_1,\ldots,\mathbf{p}'_{2N_m},s'))\right] \tag{3.6}$$

where $(\mathbf{p}_1,\ldots,\mathbf{p}_{2N_m})$ and $(\mathbf{p}'_1,\ldots,\mathbf{p}'_{2N_m})$ are the mechanical equilibrium configurations for the s and s' states, respectively. Note that these chemical state changes can occur at different monomer configurations, consistent with the idea that monomers can hydrolyze and turnover ATP at different rates at different configurations. In addition, we assume that the monomer configurations reach mechanical equilibrium much faster than the chemical transition rates. This is usually the case where protein conformation relaxation is on the order of microseconds or less. In contrast, the hydrolysis rates are on the order of $0.1s^{-1}$. Therefore, the chemical transitions occur at configurations of mechanical equilibrium in state s before the reaction occurs.

Detailed rate functions for chemical state changes have been measured for mechanoproteins such as myosin [115], but have not been measured for actin. A simple model that is consistent with the detailed balance condition is to write

$$k_{s\to s'} = k^0_{s\to s'} \exp\left[-\frac{1}{2}(E(\mathbf{p}_1,\ldots,\mathbf{p}_{2N_m},s) - E(\mathbf{p}'_1,\ldots,\mathbf{p}'_{2N_m},s') - \Delta\epsilon)/k_{\mathrm{B}}T\right] \tag{3.7}$$

and

$$k_{s'\to s} = k^0_{s'\to s} \exp\left[\frac{1}{2}(E(\mathbf{p}_1,\ldots,\mathbf{p}_{2N_m},s) - E(\mathbf{p}'_1,\ldots,\mathbf{p}'_{2N_m},s') - \Delta\epsilon)/k_{\mathrm{B}}T\right] \tag{3.8}$$

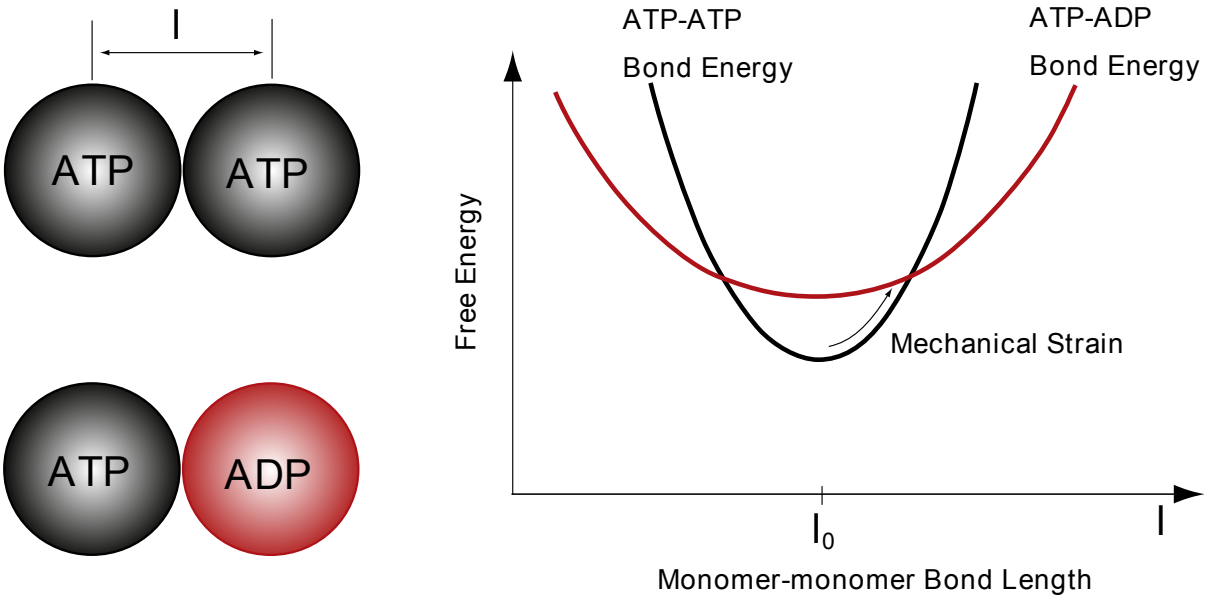

Figure 3.2: Force-induced chemical state change of monomers in actin filaments. As a schematic example, ATP-ATP bond and ATP-ADP bond energies are plotted as a function of bond length. At equilibrium, l_0, the ATP-ATP bond is favored. However, due to differences in the bond stiffness, as the bond is stretched, the ATP-ADP bond can become favorable, leading to a change in the monomer chemical state.

where $\Delta\epsilon$ is the free energy change of filament in absence of mechanical terms $U_i^{(n)}$ and $V^{(j)}$; $\Delta\epsilon = 2(\Delta G^{\text{long}}(s) - \Delta G^{\text{long}}(s')) + (\Delta G^{\text{diag}}(s) - \Delta G^{\text{diag}}(s'))$. $k^0_{s\to s'}$ is the transition rate in the absence of mechanical forces. In the absence of forces, the rate functions are evaluated at the strain-free configuration. In this case, $U_i^{(n)}$ and $V^{(j)}$ are zero, and the rates reduce to the force-free reaction rates, which obeys detailed balance:

$$\frac{k^0_{s\to s'}}{k^0_{s'\to s}} = \exp\left[-\beta\Delta\epsilon\right] \tag{3.9}$$

Note that these chemical rate functions are phenomenological. The actual rates should depend on how mechanical work changes the transition state energy of these chemical reactions. For a 1-D chain of linear springs, if ATP-ATP springs have

a different stiffness than ATP-ADP bonds, then as the strain increases, the bond energies of these states can become equal, suggesting higher probabilities of ATP-ADP conversion (Fig.3.2). If the bond stiffnesses are the same, but the bond lengths, ℓ_0, depend on the bond type, then the direction of the applied force would influence ATP to ADP conversion. Since the difference in bond energies is typically small, small forces can have significant effects on ATP conversion in actin filaments.

With these rate phenomenological functions, then it is straightforward to perform simulations of actin filament mechanical deformation and ATP hydrolysis simultaneously. We use the Gillespie algorithm to perform stochastic transitions and energy minimization to find mechanical equilibrium configurations [113]. Note that when external forces are applied to filament, energy differences between states will change, leading to faster conversion of ATP to ADP in monomers. In addition, if actin monomer bonds are allowed to break, the mechanical work done by external forces will enhance the rate of bond breakage, leading to filament rupture. The concept here is similar to fracture mechanics which also relates the rate of fracture with the total energy change.

3.2.2 Estimation of Model Parameters

To perform mechanical deformation calculations, stiffness parameters for each spring in our model are needed. We have six stiffness parameters: k_ℓ, k_θ, and k_ϕ for a longitudinal bond, and k_d, k_φ, and k_ψ for a diagonal bond. Although the free

energies of these bonds have been estimated, these stiffness parameters have not been measured. However, we can use mechanical deformation data such as stretching to determine the model parameters. Recently, Chu and Voth [83] reported the force-extension curve with coarse grained molecular dynamics (MD) model for the actin filament in both ATP and ADP states. The length of the actin filament under consideration was 0.106 μm. We used this as a reference for the comparison of stretching deformation from our model. Table 3.1 shows the stiffness parameters obtained by matching our model stretching results with the MD results.

The equilibrium configurations $(\ell_0, \theta_0, \phi_0)$ and (d_0, φ_0, ψ_0) are also potentially functions of monomer chemical state. This would imply that ATP-actin filament would have a slightly different conformation than ADP-actin filament. From crystal structure as well as cryo-electron microscopy studies, there is no evidence that the global filament shape depends on monomer chemical state. Therefore we assume these parameters are constants.

The mechanical model here is similar to the work in [89] which defines a biopolymer using single monomers and their interactions. However, while [89] derives mechanical parameters from microscopic data (bond stiffness, subunit interface area and geometry), in the current work we obtain these parameters from global mechanical properties of a filament. To investigate the possible significant effects of the choice of parameters, we performed sensitivity analysis of filament deformation as a function of changes in mechanical parameters (Table3.2). For the stretching case 400 pN, and

Table 3.2: Percent change in bending and stretching strain due to 1 percent perturbations on the stiffness parameters

	k_ℓ	k_θ	k_ϕ	k_d	k_φ	k_ψ
F-ATP Bend	0.91	0.31	5.72	0.09	0.04	0.18
F-ATP Stretch	9.04	0.08	0.13	0.16	0.04	0.60
F-ADP Bend	0.84	0.26	4.37	0.12	0.05	0.19
F-ADP Stretch	9.21	0.08	0.12	0.10	0.04	0.49

for the bending case 10 pN force were applied as explained in the previous section. The filament length in the simulation is 0.232 μm. We perturbed each parameter by increasing or decreasing individually by 1 % to obtain the average percent changes. In case of stretching, the linear spring of the longitudinal bond, k_ℓ, is the most sensitive and the second sensitive is k_ψ. In case of bending, one of angular springs k_ψ in the diagonal bond is the most sensitive and k_ℓ is the second sensitive. This applies regardless of the chemical state of monomers. From this, one can see that the linear spring in the longitudinal bond is important in the mechanical response to external forces. When it comes to pure twist, one can infer that k_θ will contribute the most.

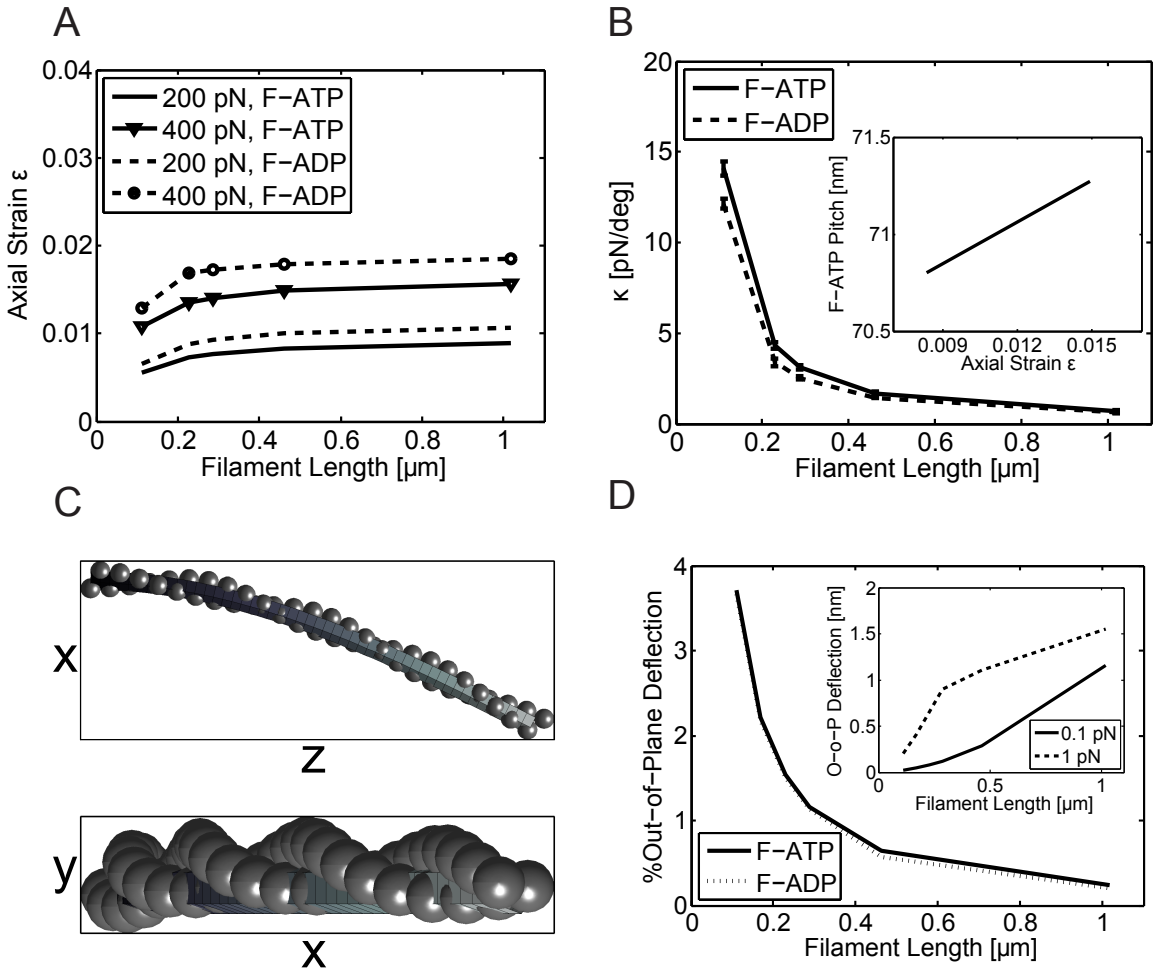

Figure 3.3: Mechanical properties of an actin filament according to the coarse-grained model. (A) Stretching strain as a function of force, f, filament length and filament type, F-ATP (solid lines) or F-ADP (dotted lines). (B) κ, stiffness of filament twist-stretch coupling, is shown as a function of filament length, F-ATP (solid lines), F-ADP (dotted lines). Shown in inset is the increase of average pitch of $0.46\mu m$ long filament as a function of stretching strain. (C) Bent configuration of a $0.145\mu m$ F-ATP and the best fit 2D ($x-z$ plane) thin rod as seen from two different viewing angles. Applied bending force is in x-direction with a magnitude of 4 pN. (D) Percent contribution of the out-of-plane filament tip deflection to the overall tip deflection due to bending as a function of filament length. Applied bending force is 0.2 pN. F-ATP (solid lines), F-ADP (dotted lines). Inset shows the amount of out-of-plane tip deflection for different filament lengths and bending forces, 0.2 pN (solid line), 4 pN (dashed line).

3.3 Results

3.3.1 Model Predictions of F-actin Deformation Under Load

We utilize our F-actin model to investigate mechanical deformation as a function of the applied force. Stretching and bending deformation calculations are performed for varying filament lengths and applied forces. In each calculation, we consider changes in the chemical state of the monomer: i.e., where all the monomers are either in ATP or ADP states, respectively.

In Fig.3.3A, the equilibrium strain, $\epsilon = (l - l_0)/l_0$, as a function of stretching force f is plotted for several different forces and lengths. As expected, an actin filament with ADP in the catalytic site is softer than with ATP. We find that ϵ is a linear function of the applied force for up to $f = 200$ pN. The stretching modulus can be computed by analyzing the strain as a function of force. We find that the modulus is $\mu = 250MPa$. In cases where there are a mixture of ATP and ADP monomers in the filament, the modulus is also well described by an interpolation relationship: $\mu = x\mu_{ATP} + (1 - x)\mu_{ADP}$, where x is the fraction of ATP monomers.

While F-actin is quite stiff under stretch, because it is helical, stretching deformation is naturally coupled to filament twist. This coupling has been discussed as a possible mechanism of mechanosensation [74]. We define κ as the stretch-twist cou-

pling parameter: $f = \kappa\Theta$, where f is the magnitude of the stretching force and Θ is the induced twist at the end of the filament. Fig.3.3B shows κ as a function of filament length, L. The error bars represent results from different stretching forces (20, 100, 200, 400 pN). The plotted relationship obeys the power law $\kappa \sim L^b$ where b is around -3/2. In the inset of Fig.3.3B, we see that the F-actin pitch also changes (shown for 0.46 μm ATP filament) as a function of stretching strain. These results indicate that a helical structure must naturally couple twist with the tension in the filament. If there are actin-associated proteins bound on the filament, binding kinetics and conformations of these proteins would be affected by tension. This could be another underlying mechanism during cellular mechanosensation where actin filaments are pulled by myosin motors in stress-fibers.

A helical structure such as F-actin will also respond with out-of-plane bending when a force is applied perpendicular to the filament. This is caused by bend-twist coupling, which is also common in other helical bundles such as the coiled coil [50]. Using a different model, the twist-bend coupling length of F-actin was predicted to be 0.4 μm [89]. This result can be compared to the elastic thin rod theory which is a standard methodology in defining mechanical properties of biofilaments. Fig.3.3C shows the bending geometry of a 0.145 μm ATP actin filament and the best thin rod theory comparison. In Fig.3.3D, we quantify the out-of-plane deflections in terms of filament length, amount of bending force and monomer chemical state. From our results, we see that the thin rod theory predicts no out-of-plane bending and therefore

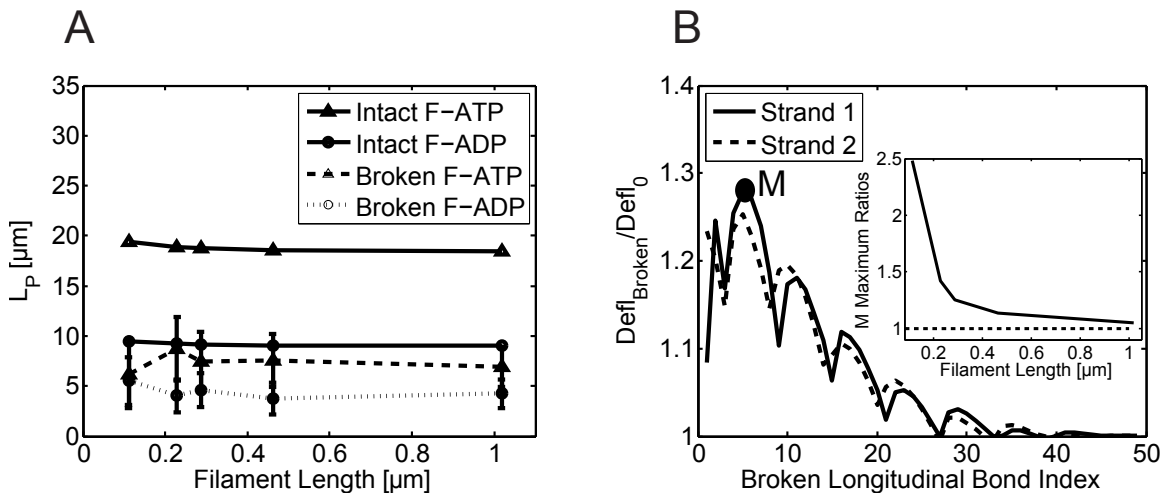

Figure 3.4: Persistence length L_p derived from the mechanical model and the effect of broken bonds. (A) L_p prediction obtained from fitting thin rod theory to deformations in intact filaments (solid lines). Dotted lines with errorbars represent the mean and standard deviation in L_p for filaments with randomly broken bonds (see text for details). All the filaments are bent under 1 pN force. Different chemical states of the filaments are denoted as F-ATP (triangles) and F-ADP (circles). (B) The ratio of bending deflection of a filament with a broken longitudinal bond at a particular index (abscissa) to the deflection of an intact filament. Filament length is $0.29\mu m$ and bent under 4 pN.

is not an accurate model for short actin filaments. For long filaments ($> 1\mu$m), the out-of-plane bending is less important. The inset of Fig.3.3D shows that the amount of out-of-plane deflection levels out once a critical filament length and bending force are reached.

3.3.2 Bending persistence length and effects of broken bonds

Bending properties of F-actin is important for understanding the mechanical behavior of the cellular cytoplasm and the dynamics of actin network remodeling under force [61]. In the cell, actin filaments also experience forces from membranes and other proteins, as well as forces from thermal fluctuations [99]. Therefore, it is possible that some of the bonds in the filaments are broken. In addition, monomers in the filament can be either in ATP or ADP states. From the bending simulation results, we can estimate the bending persistence length, L_p, by comparing the bending results of our model with those from the elastic thin rod theory. This comparison serves as a verification of our model and enables us to explore the role of broken bonds and filaments with different monomer chemical states in determining the overall actin network mechanics.

Fig.3.4A shows the obtained bending persistence length values of F-actin with different structural conditions. The obtained persistence lengths of an intact F-ATP and intact F-ADP under 1 pN force are in good agreements with the reported values [58, 59], 16 $\sim$ 9 μm. Note that due to helical nature of the filament, there is some length dependence in L_p. In the second set of the simulations, 5% of all the bonds in the filament are randomly broken. This calculation is repeated 20 times and bending data are averaged. The corresponding error bars for ATP and ADP

filaments are shown in Fig.3.4A. As the portion of broken bonds increases, the mean persistence length decreases and the standard deviation increases (data not shown). Note that we compute the persistence length from the comparison of the bending deflection (tip-to-tip vector) projected onto the plane of the applied force because thin rod theory predicts the shape of a filament only in 2D (See Fig.3.3C). Strictly speaking, if we include out-of-plane deflection due to the bend-twist coupling effect, the corresponding persistence length would be slightly lower than the values shown. However, bend-twist coupling is not significant in longer filaments and therefore is ignored.

The physical location of the broken bond on a filament also strongly influences the overall bending of the filament under force. In Fig.3.4B, we show the ratio of the bending deflection of a 0.29 μm filament under 4 pN with a broken longitudinal bond at a particular index of one strand to the deflection of an intact filament. We observe that broken bonds that are closer to the fixed boundary increase the amount of bending deflection. The effect of the location of the broken bonds on bending also diminishes as filament length increases. We do not observe any significant difference due to breaking of diagonal bonds.

Table 3.3: Model parameters for bonds in a Cofilactin filament

Parameter	Value
ℓ_0 [nm]	6.20
θ [°]	34.94
ϕ [°]	-9.34
d_0 [nm]	6.00
φ_0 [°]	107.47
ψ_0 [°]	58.80

3.4 Influence of Actin Binding Proteins

In the cell, a large number of actin binding proteins (ABPs) interact with the filament network and alter the biochemical and mechanical state of the network. Our model can be used to investigate the influence of actin binding proteins on the filament structure. There have been studies of ABPs interacting with actin using MD. In our modeling approach, we can describe the role of ABPs by considering how these proteins can change structural parameters such as $(\ell_0, \theta_0, \phi_0)$ and/or stiffness parameters $(k_\ell, k_\theta, k_\phi)$ for each monomer. Binding of a single ABP can potentially change these parameters for the bound actin, and these local changes can be amplified to global changes in the actin structure.

Changes in the F-actin pitch upon ABPs binding has been observed experimentally [92, 116]. ADF/Cofilin is an important ABP whose cellular function is to sever

actin filaments by introducing local mechanical deformations. Cofilin binds between two actin monomers and affects the actin-actin longitudinal bond. Therefore, its function can be modeled by changing the longitudinal bond parameters while leaving the diagonal bond unchanged [93]. To obtain the change in ℓ_0 in response to cofilin binding, we can consider the relationship between the helical pitch and the helical contour length while keeping the filament length and radius fixed. A helical contour is described by the vector $\mathbf{r}(t) = (r_0 \cos at, r_0 \sin at, bt)$ where the contour length t ranges from $[0, L]$; $a = 1/(r_0^2 + (P/2\pi)^2)^{1/2}$, $b = (P/2\pi)/(r_0^2 + (P/2\pi)^2)^{1/2}$ and P is the helical pitch. If the contour length changes from t to t', the changes in the filament length is given by $\sqrt{g}b'L - bL$, where $\partial t'/\partial t = \sqrt{g}$ is the change in helical contour length, and b' is obtained with the new pitch P'. Since cofilin does not appear to change the filament length, we can solve for $\sqrt{g}$ and P' using the equation $\sqrt{g}b'L - bL = 0$. Fig.3.5A shows the solution of this equation plotted as $\sqrt{g}$ vs. P'. This result suggests that the new actin-actin bond length with cofilin, ℓ_0', is approximately 1% longer, and the pitch of the cofilin decorated filament is roughly 60nm.

In addition to a change in ℓ_0, [117] also showed that upon binding of cofilin, actin monomers tilt towards the helical contour axis by 6-12°. This corresponds to a modification of ϕ_0 in our model. Table 3.3 shows the model parameters for the cofilin modified actin-actin longitudinal bond. Fig.3.5B shows the overall filament conformation with a number of monomers decorated with cofilin. As noted by recent

studies [95], we observe that maximum strain occurred at the boundaries between decorated and non decorated monomers. Finally, Fig.3.5C shows the possible cooperativity when 2 cofilins are bound to the same filament. As cofilin changes the bond parameters of a single longitudinal bond, it induces local mechanical strain on the neighboring bonds. We can compute the total strain energy of the filament as a function of distance between 2 bound cofilins. We define ΔE as the difference between the energy of a single filament with 2 cofilins and 2 times the energy of the filament with one cofilin. This difference can be thought of as a cooperative binding energy.

Fig. 3.5C shows that this cooperativity is generally favorable when 2 cofilin molecules are in the near vicinity. The degree of cooperativity decreases as the distance between two cofilins increases. Also, we observe that there is anticooperativity beyond two second nearest neighbor cofilins (i and $i \pm 2$). Another way to understand the action of cofilin is that it introduces a local mechanical defect; these defects can interact over long distances, leading to anticooperativity. Note that by stretching the actin-actin bond, cofilin also catalyzes conversion from ATP-actin to ADP (see next section). This leads to eventual filament severing.

Arp2/3 is another actin binding protein whose main cellular function is to nucleate new filaments by creating a branch from an existing filament. A recent study [97] showed that Arp2/3 preferentially binds to the convex side of a curved filament confined on a 2D surface. They explained this phenomena by treating the actin filament as a structureless rod and considering curvature fluctuations of the filament. They

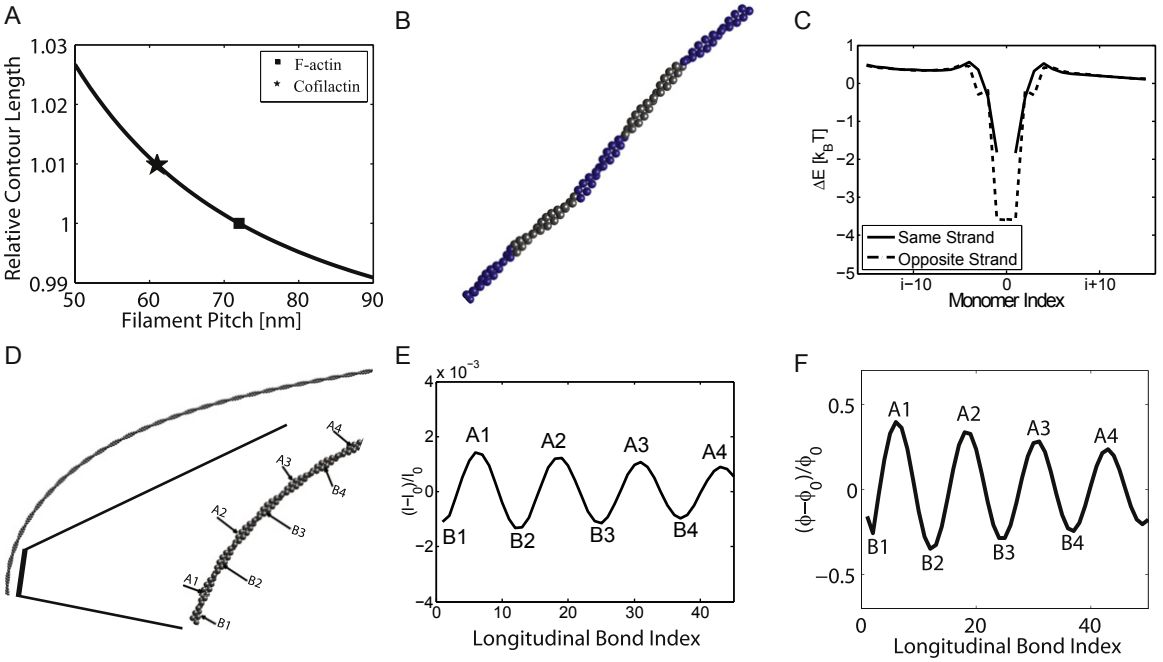

Figure 3.5: Influence of actin binding proteins. (A) The stretch (or compression) strain in the longitudinal bond lengths, l, for a fixed filament length and radius (see text). The stretching strain is shown as a function of changing pitch. (B) conformation of a 0.29 μm actin filament partially decorated with cofilin in a banded manner. Blue monomers are decorated with cofilin. (C) Cooperative binding energy for a filament with 2 bound cofilins (see text). The cooperative energy is plotted as a function of relative positions (in terms of actin monomer index) of the cofilins. (D) Conformation of a 1.01 μm F-ATP bent under 0.5 pN. (E) Longitudinal bond strains of the filament shown in D. (F) Angular strain on the longitudinal bonds of the filament shown in D. In both (E) and (F), the peaks and valleys labeled by A_i and B_i corresponds to the outer in inner positions labeled in D.

proposed that Arp2/3 prefers to bind to highly curved configurations, and bending biases the curvature fluctuation. Within our model, actin is a double helix, and without considering fluctuations, we can examine the equilibrium structure when the filament is curved. Specially, we can examine the strains in the actin-actin bonds when the filament is curved. Fig.3.5D shows a 1.01 μm F-ATP bending under 0.5 pN. Fig.3.5E and F show the linear and angular strain in the bonds in the bent structure shown in Fig.3.5D. The results show that the strain in the inner strand (measured with respect to positive curvature as shown in Fig.3.5D inset) is different than the outer strand. This result is obtained for mechanical equilibrium structures without considering fluctuations. It arises because of helical nature of F-actin. Arp2/3 could potentially bind between actin monomers with positive strain, and therefore preferentially bind on the outer strand of positively curved filaments.

3.5 Force-induced Chemical State Change and Mechanosensation

In earlier results, we showed that the mechanical properties of F-actin depends on the hydrolysis state of the monomers. ATP-actin, even though is structurally very similar to ADP-actin, at the filament level is slightly stiffer. The consequence of such a mechanical difference is that externally applied forces can alter the chemical state of monomers in the filament. The basic concept is shown in Fig.3.2. If the

bond energy is plotted as a function of the monomer-monomer bond length, then the equilibrium length, l_0, is identical for ATP-ATP bond vs. ATP-ADP bond. The free energy difference of ATP-ADP bond is taken to be as higher by $2k_{\mathrm{B}}T$. (Other energy differences can be used as well, and would change the quantitative influence of force on actin chemistry.) As a force is applied and l increases away from l_0, the difference in the curvature of the energy landscape will lead to a crossing point. At this point, ATP-ATP bond has the same free energy as the ATP-ADP bond, therefore the probability of converting one of the monomers to ADP is enhanced. As l increases further, the ADP-actin state becomes more favorable. Thus, the equilibrium between ATP and ADP states (actually ADP.Pi and ADP states) is influenced by forces and changes in the mechanical energy. In the Model section, we discussed a simple model to modify the rate constants while preserving detailed balance. The actual rates may differ quantitatively, but the overall effect must remain the same.

Using the Gillespie stochastic simulation algorithm, we computed ATP-actin filaments under bending forces up to 60 pN and stretching forces up to 600 pN and allow the monomers to change their chemical state. As forces are applied, the individual monomers stochastically change their chemical state according to rate constants defined in Eqs.3.7 and 3.8. The rate constant, $k^0_{s\to s'}$, has been estimated [15]. Here we report the equilibrium result as the simulation time approaches infinity. Fig.3.6A shows the average stretching strain for a 112 nm long filament under different pulling forces. Due to high stretching stiffness, the amount of strain buildup on the filament

is very small. This is the reason of why there is not a significant amount of chemical state conversion into ADP. As the pulling force is increased, the monomers increasingly convert to ADP. Eventually, at 600pN, all of the monomers are essentially in ADP state. Note that our model currently does not allow the filaments to rupture. It is likely that filaments would have a high probability of breaking before the filament fully converts. Fig.3.6B shows the bending deformations while the chemical states of the monomers are changing. We see that if monomers are allowed to convert to ADP, the bending stiffness decreases as a function of applied force. This observation could potentially explain the reversible stress softening behavior of F-actin [118]. Fig.3.6A and B also show the average chemical state of the filament under force with a color code (between red and green). For the bending case, together with Fig.3.3F, we can conclude that the monomers under highest strain are closest to the left end which is fixed. This is the reason why ADP rich monomers tend to appear in those locations. Note that the magnitude of the bending forces can be quite low. At 20pN, there is already a significant amount of conversion to ADP. For longer filaments (Fig.3.6C), smaller bending forces are needed to induce chemical state change because of the larger mechanical work done.

The results presented in Fig. 3.6 do depend on the choice of $\Delta\epsilon$, the difference in bond free energies of ATP and ADP states. As an alternative, we may consider a different parameter set in Table 3.1 with different relative magnitudes of diagonal and longitudinal bonds. For example, a smaller $\Delta\epsilon$ would lead to increasing populations

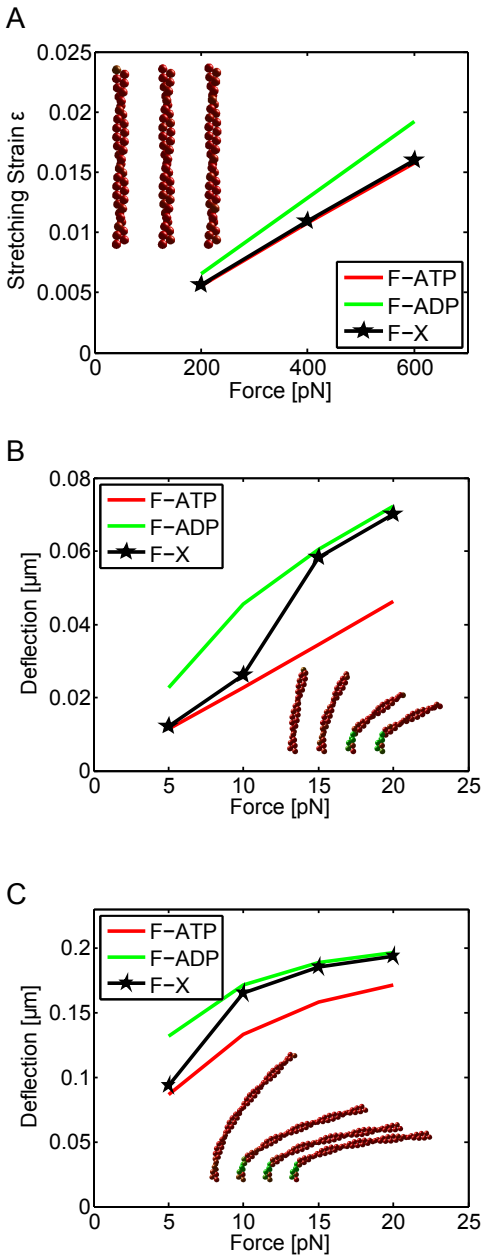

Figure 3.6: Loading force-induced chemical state change of monomers in actin filaments. (A) Stretching induced changes in the monomer chemical state as a function of force. The filament length is $0.11\mu m$. (B and C) Bending induced changes in the monomer chemical state as a function of force. In (B), the filament length is $0.9\mu m$ and in (C) the filament length is doubled, $0.17\mu m$. In all figures, the average conformation of filaments that correspond to a particular force are compared with filaments with all ATP or all ADP. We see that for a longer filament, changes in chemical states are more dramatic for the same force.

of ADP subunits [119].

3.6 Discussion and Conclusion

We have introduced a mechanochemical model of actin filaments by explicitly considering the bonding interaction between actin monomers. The filament is described as two helical strands connected by longitudinal and diagonal bonds. The chemical state of the actin monomers can change, and the rate of ATP conversion depends on the overall elastic energy of the filament. As expected, we find actin filaments are mechanically stiff under stretch, but deform easily under bending forces. The model shows that for filament length much longer than the helical actin pitch ($> 1\mu$m), the filament mechanically deforms as a semi flexible rod. However, the mechanical behavior depends on the chemical state of actin. ADP-actin filaments are softer than ATP-actin. The model is also able to capture aspects of actin accessory proteins interacting with the filament.

The model uses a coarse-grained description of actin monomer mechanics, and does not consider internal conformational complexity of actin, although it does include possible conformational changes due to ATP hydrolysis. Therefore, it is an intermediate scale model in between atomistic scale and the network scale. Internal conformational complexity can also be partially captured using nonlinear mechanical models. Here, simple harmonic spring-like functions are assumed for monomer-monomer interaction

with no coupling between kinematic variables. This is the simplest model that still reproduces the essential features of actin filament mechanics. More sophisticated models can be made, but would require increased number of parameters. Nevertheless, the model parameters can be obtained from molecular dynamics simulations, or fitting to experimental data. Further studies on the model parameters would improve model predictions.

In this model, we examined chemical state change from ATP-actin to ADP-actin. There are in fact many more possible chemical states, and this could underlie the mechanochemical complexity of actin networks. For instance, after ATP is hydrolyzed to ADP, the monomer can release inorganic phosphate and break the existing actin-actin bond, especially when the filament is under high mechanical load. This can lead to filament rupture. Actin filament rupture has been studied experimentally with single filaments [120]. It was found that when the radius of curvature of the filament is less than 300nm, the rupture probability increases. Also, using simple force balance considerations in a nerve growth cone, a recent study [121] has estimated the forces on a steady-state actin treadmill and showed the importance of filament rupture in resistance to retrograde flow. The framework used in this work can be extended to describe such situations.

By understanding the full range of mechanochemical behavior of actin, improved models of actin's role in the cell can be made. For instance, to understand cortical actin network contraction and stress-induced softening seen in experiments, chemical

state changes and turnover of actin monomers in response to forces must be examined. Our model is first such model in this direction. Extrapolating to the network scale, these mechanochemical effects will significantly influence the viscoelasticity of the network. Combined with nucleation, growth, contraction and turnover of the network, a quantitative model of the cellular cytoplasm can be developed. Note that these mechanochemical effects may lead to unique network properties that are not present in static polymer networks where bonds between monomers are essentially permanent. Therefore, new physics may be present and could lead to surprising mechanistic insights for the cell.

Chapter 4

Conclusions

4.1 Summary

In Chapter 2, we examined the mechanical responses of typical coiled coils, and built a coarse-grained mechanical model to describe the conformations of the protein under different load configurations.

Using molecular dynamics simulations we applied bending forces onto different length coiled coil molecules. We observed that during bending a coiled coil molecule deflects out of the plane of the applied force. This is due to the helical structure of constituent alpha helices and the coiled structure of the coiled coil molecule. We demonstrate that our model when bent can capture this bend-twist coupling. The continuum thin rod theory result cannot capture this out of plane bending phenomenon. Also, our bending results are a better fit to MD results than our predecessor WS

model.

In order to extract the bending persistence length of our coiled coil molecule, we first fitted the critical buckling force data coming from thin rod theory prediction. The best fitting bending persistence length was 200 nm, twice that of individual alpha helices. After that, we compared our coiled coil bending deflection results with the thin rod theory prediction. Our comparison showed that the deflection predictions are not simply matching even though we are using the same single bending persistence parameter. This mismatch and bend-twist coupling behavior suggest that coiled coil mechanical response cannot be fully characterized by a single parameter.

Next, using molecular dynamics simulations we extracted twist persistence length of different length coiled coil molecules. On average the twist persistence length is 100 nm, twice that of single alpha helices. We observed that the twist persistence length slightly decreases as a function of the coiled coil length. Twist persistence length of our model is about 100 nm, as well. However, the predecessor WS model coiled coil twist persistence prediction is around 160 nm. We think this result is reasonable as the WS model assumes that the hydrophobic bonds are rigid, thus harder to twist

Finally, using our model we simulated the situation of sliding of one alpha helix in the coil while the other is fixed. We observed that a small sliding motion is conformationally amplified and caused the coiled coil to make a very significant bending response at the other end of the coil. The cost to introduce this sliding motion is within the range of the energy brought in by a small molecule binding to a filament.

This conformational amplification behavior was found to be increasing as a function of coiled coil length.

In Chapter 3, we described our mechanochemical model of F-actin. We quantified single F-actin mechanical behavior depending on the monomer chemical states, filament length, the type of the applied forces and broken bonds. Firstly, we tested the F-Actin model under stretching and found that the strain is close to the experimental findings. We observed that when stretched, the filament tip twists. This tip twist increases as a function of the filament length.

Secondly, just like in the case of coiled coil, F-actin has out of plane bending and our model captures that behavior. We found that the amount of out of plane deflection decreases as the filament length increases. To check the effect of the broken bonds on the bending response, we randomly broke 5 percent of all the bonds in different length F-actin molecules. Our results showed that the introduction of broken bonds significantly decreased the bending stiffness of F-actin. We also observed that breaking longitudinal bonds decreases filament bending stiffness more than the diagonal bonds.

Thirdly, we simulated the working principles of two actin binding proteins, ARP2/3 and cofilin. Cofilactin has a different helical geometry than bare actin filaments. Using this information we modelled a cofilactin filament and brought a new angle to the cooperativity of cofilin assembly around F-actin. Our model also brings a possible explanation of the preferential binding of ARP2/3 and can predict the exact locations

of where F-actin would branch by ARP2/3.

Finally, using our mechanochemical model we showed that under physiological conditions under stretching, it is very hard for an ATP-F-actin filament to convert the ATP molecules into ADP molecules. However, during bending there is enough mechanical strain on the bonds to make chemical conversion to ADP. We also observed that it takes a bigger amount of load for short filaments to convert ATP to ADP in comparison with longer filaments.

4.2 Future Outlook

The main advantage of our proposed models over the atomistic simulations is their speed. One possible extension of our models would be going one length scale up and using the models to efficiently simulate the network/bundle behavior of filaments. Another advantage of our models is their capability of simulating the effect of local perturbations on the global filament response. In our coiled coil model we have demonstrated this with helix sliding. There are several such biologically relevant nonlinear perturbations and our model may be a proper tool to study and understand mechanical response of biofilaments. Also, in our coiled coil study, we only reported the results of the model with regularly repeated hydrophobic interactions. Nature is full of irregularities. Our model might be used to understand the global effect of such irregular interactions as well. In our actin model we dealt with two actin binding

proteins only, but our model is flexible enough to study other binding partners, tool.

Actin polymerization is an important area of study. In our model, we assumed that there is no polymerization and solely focused on the mechanical response of the filament. Although introduction of polymerization into our simulations is not hard, we note that this would increase the simulation times by increasing the filament lengths and number of possible destination states. In addition to actin, our mechanochemical model framework might be used to study other mechanosensitive structures. One such structure is the focal adhesion complex (FAC). To make a mechanochemical model of FAC however one needs to take into account the addition or deletion of new monomers into the complex.

Bibliography

[1] P. R. Cavanagh, A. A. Licata, and A. J. Rice, "Exercise and pharmacological countermeasures for bone loss during longduration space flight," *Gravitational and Space Biology*, vol. 18, no. 2, 2007.

[2] P. Kanchanawong, G. Shtengel, A. M. Pasapera, E. B. Ramko, M. W. Davidson, H. F. Hess, and C. M. Waterman, "Nanoscale architecture of integrin-based cell adhesions," *Nature*, vol. 468, no. 7323, pp. 580–584, 2010.

[3] B. Geiger, J. P. Spatz, and A. D. Bershadsky, "Environmental sensing through focal adhesions," *Nature Reviews Molecular Cell Biology*, vol. 10, no. 1, pp. 21–33, 2009.

[4] A. J. Engler, S. Sen, H. L. Sweeney, and D. E. Discher, "Matrix elasticity directs stem cell lineage specification," *Cell*, vol. 126, no. 4, pp. 677–689, 2006.

[5] J. Swift, I. L. Ivanovska, A. Buxboim, T. Harada, P. D. P. Dingal, J. Pinter, J. D. Pajerowski, K. R. Spinler, J.-W. Shin, M. Tewari *et al.*, "Nuclear lamin-a

scales with tissue stiffness and enhances matrix-directed differentiation," *Science*, vol. 341, no. 6149, p. 1240104, 2013.

[6] W. Xu, R. Mezencev, B. Kim, L. Wang, J. McDonald, and T. Sulchek, "Cell stiffness is a biomarker of the metastatic potential of ovarian cancer cells," *PloS one*, vol. 7, no. 10, p. e46609, 2012.

[7] S. Suresh, "Biomechanics and biophysics of cancer cells," *Acta Materialia*, vol. 55, no. 12, pp. 3989–4014, 2007.

[8] A. Noy, *Handbook of molecular force spectroscopy*. Springer, 2008.

[9] E. Kim, W. Wriggers, M. Phillips, K. Kokabi, P. A. Rubenstein, and E. Reisler, "Cross-linking constraints on f-actin structure," *Journal of molecular biology*, vol. 299, no. 2, pp. 421–429, 2000.

[10] Y. Nikolaev and K. Pervushin, "Rethinking leucine zipper– a ubiquitous signal transduction motif," *Nature Precedings*, vol. http://precedings.nature.com/documents/3271/version/1, no. Accessed August 6, 2010, 2009.

[11] R. Fraser and T. MacRae, *Conformation in fibrous proteins and related synthetic polypeptides*. Elsevier, 1973.

[12] A. N. Lupas and M. Gruber, "The structure of α-helical coiled coils," *Advances in protein chemistry*, vol. 70, pp. 37–38, 2005.

[13] J. M. Fletcher, R. L. Harniman, F. R. Barnes, A. L. Boyle, A. Collins, J. Mantell, T. H. Sharp, M. Antognozzi, P. J. Booth, N. Linden *et al.*, "Self-assembling cages from coiled-coil peptide modules," *Science*, vol. 340, no. 6132, pp. 595–599, 2013.

[14] H. Gradišar, S. Božič, T. Doles, D. Vengust, I. Hafner-Bratkovič, A. Mertelj, B. Webb, A. Šali, S. Klavžar, and R. Jerala, "Design of a single-chain polypeptide tetrahedron assembled from coiled-coil segments," *Nature chemical biology*, vol. 9, no. 6, pp. 362–366, 2013.

[15] I. Fujiwara, D. Vavylonis, and T. D. Pollard, "Polymerization kinetics of adp-and adp-pi-actin determined by fluorescence microscopy," *Proceedings of the National Academy of Sciences*, vol. 104, no. 21, pp. 8827–8832, 2007.

[16] C. W. Wolgemuth and S. X. Sun, "Elasticity of α-helical coiled coils," *Physical review letters*, vol. 97, no. 24, p. 248101, 2006.

[17] R. Capovilla, C. Chryssomalakos, and J. Guven, "Hamiltonians for curves," *Journal of Physics A: Mathematical and General*, vol. 35, no. 31, p. 6571, 2002.

[18] K. C. Wolfe, W. A. Hastings, S. Dutta, A. Long, B. A. Shapiro, T. B. Woolf, M. Guthold, and G. S. Chirikjian, "Multiscale modeling of double-helical dna and rna: a unification through lie groups," *The Journal of Physical Chemistry B*, vol. 116, no. 29, pp. 8556–8572, 2012.

[19] M. Moakher and J. H. Maddocks, "A double-strand elastic rod theory," *Archive for rational mechanics and analysis*, vol. 177, no. 1, pp. 53–91, 2005.

[20] T. Bornschlögl and M. Rief, "Single-molecule dynamics of mechanical coiled-coil unzipping," *Langmuir*, vol. 24, no. 4, pp. 1338–1342, 2008.

[21] Y. Tsuda, H. Yasutake, A. Ishijima, and T. Yanagida, "Torsional rigidity of single actin filaments and actin–actin bond breaking force under torsion measured directly by in vitro micromanipulation," *Proceedings of the National Academy of Sciences*, vol. 93, no. 23, pp. 12 937–12 942, 1996.

[22] S. X. Sun, G. Lan, and E. Atilgan, "Stochastic modeling methods in cell biology," *Methods in cell biology*, vol. 89, pp. 601–621, 2008.

[23] J. Symersky, A. Perederina, M. N. Vassylyeva, V. Svetlov, I. Artsimovitch, and D. G. Vassylyev, "Regulation through the rna polymerase secondary channel structural and functional variability of the coiled-coil transcription factors," *Journal of Biological Chemistry*, vol. 281, no. 3, pp. 1309–1312, 2006.

[24] F. Corrêa, C. S. Farah, and R. K. Salinas, "Mg2+ ions bind at the c-terminal region of skeletal muscle α-tropomyosin," *Biopolymers*, vol. 91, no. 7, pp. 583–590, 2009.

[25] M. D. Baker, P. M. Wolanin, and J. B. Stock, "Signal transduction in bacterial chemotaxis," *Bioessays*, vol. 28, no. 1, pp. 9–22, 2006.

[26] O. D. Testa, E. Moutevelis, and D. N. Woolfson, "Cc+: a relational database of coiled-coil structures," *Nucleic acids research*, vol. 37, no. suppl 1, pp. D315–D322, 2009.

[27] F. Crick, "Is α-keratin a coiled coil?" *Bioessays*, vol. 170, no. 1, pp. 882–883, 1952.

[28] J. Liu, Q. Zheng, Y. Deng, C.-S. Cheng, N. R. Kallenbach, and M. Lu, "A seven-helix coiled coil," *Proceedings of the National Academy of Sciences*, vol. 103, no. 42, pp. 15 457–15 462, 2006.

[29] J. Seo and C. Cohen, "Pitch diversity in α-helical coiled coils," *Proteins: Structure, Function, and Bioinformatics*, vol. 15, no. 3, pp. 223–234, 1993.

[30] G. N. Phillips, "What is the pitch of the α-helical coiled coil?" *Proteins: Structure, Function, and Bioinformatics*, vol. 14, no. 4, pp. 425–429, 1992.

[31] B. Busson and J. Doucet, "Modeling alpha-helical coiled coils: analytic relations between parameters," *Journal of structural biology*, vol. 127, no. 1, pp. 16–21, 1999.

[32] S. Neukirch, A. Goriely, and A. C. Hausrath, "Chirality of coiled coils: elasticity matters," *Physical review letters*, vol. 100, no. 3, p. 038105, 2008.

[33] I. Adamovic, S. M. Mijailovich, and M. Karplus, "The elastic properties of the structurally characterized myosin ii s2 subdomain: a molecular dynamics and

normal mode analysis," *Biophysical journal*, vol. 94, no. 10, pp. 3779–3789, 2008.

[34] S. Sadeghi and E. Emberly, "Length-dependent force characteristics of coiled coils," *Physical Review E*, vol. 80, no. 6, p. 061909, 2009.

[35] S. K. Lakkaraju and W. Hwang, "Critical buckling length versus persistence length: what governs biofilament conformation?" *Physical review letters*, vol. 102, no. 11, p. 118102, 2009.

[36] R. J. Hawkins and T. C. McLeish, "Dynamic allostery of protein alpha helical coiled-coils," *Journal of The Royal Society Interface*, vol. 3, no. 6, pp. 125–138, 2006.

[37] C. A. Laughton, B. F. Luisi, J. V. Pratap, and C. R. Calladine, "A potential molecular switch in an α-helical coiled coil," *Proteins: Structure, Function, and Bioinformatics*, vol. 70, no. 1, pp. 25–30, 2008.

[38] A. P. Carter, J. E. Garbarino, E. M. Wilson-Kubalek, W. E. Shipley, C. Cho, R. A. Milligan, R. D. Vale, and I. Gibbons, "Structure and functional role of dynein's microtubule-binding domain," *Science*, vol. 322, no. 5908, pp. 1691–1695, 2008.

[39] T. Kon, K. Imamula, A. J. Roberts, R. Ohkura, P. J. Knight, I. Gibbons, S. A. Burgess, and K. Sutoh, "Helix sliding in the stalk coiled coil of dynein couples

atpase and microtubule binding," *Nature structural & molecular biology*, vol. 16, no. 3, pp. 325–333, 2009.

[40] L. L. D. Landau and E. E. M. Lifshits, *Theory of Elasticity, Course of theoretical Physics vol VII, 3rd revised edition.* London: Butterworth-Heinemann, 1995.

[41] S. Choe and S. X. Sun, "The elasticity of α-helices," *The Journal of chemical physics*, vol. 122, p. 244912, 2005.

[42] W. Humphrey, A. Dalke, and K. Schulten, "Vmd: visual molecular dynamics," *Journal of molecular graphics*, vol. 14, no. 1, pp. 33–38, 1996.

[43] M. T. Nelson, W. Humphrey, A. Gursoy, A. Dalke, L. V. Kalé, R. D. Skeel, and K. Schulten, "Namd: a parallel, object-oriented molecular dynamics program," *International Journal of High Performance Computing Applications*, vol. 10, no. 4, pp. 251–268, 1996.

[44] A. D. MacKerell, N. Banavali, and N. Foloppe, "Development and current status of the charmm force field for nucleic acids," *Biopolymers*, vol. 56, no. 4, pp. 257–265, 2000.

[45] T. Darden, D. York, and L. Pedersen, "Particle mesh ewald: An n log (n) method for ewald sums in large systems," *The Journal of chemical physics*, vol. 98, p. 10089, 1993.

[46] I. MathWorks, *MATLAB: the language of technical computing. Desktop tools and development environment, version 7*. MathWorks, 2005, vol. 9.

[47] C. Chothia, M. Levitt, and D. Richardson, "Helix to helix packing in proteins," *Journal of molecular biology*, vol. 145, no. 1, pp. 215–250, 1981.

[48] M. Bathe, C. Heussinger, M. M. Claessens, A. R. Bausch, and E. Frey, "Cytoskeletal bundle mechanics," *Biophysical journal*, vol. 94, no. 8, pp. 2955–2964, 2008.

[49] G. Lan and S. X. Sun, "Flexible light-chain and helical structure of f-actin explain the movement and step size of myosin-vi," *Biophysical journal*, vol. 91, no. 11, pp. 4002–4013, 2006.

[50] O. N. Yogurtcu, C. W. Wolgemuth, and S. X. Sun, "Mechanical response and conformational amplification in α-helical coiled coils," *Biophysical journal*, vol. 99, no. 12, pp. 3895–3904, 2010.

[51] S. A. Chervitz and J. J. Falke, "Molecular mechanism of transmembrane signaling by the aspartate receptor: a model," *Proceedings of the National Academy of Sciences*, vol. 93, no. 6, pp. 2545–2550, 1996.

[52] W. Y. Edward and D. E. Koshland, "Propagating conformational changes over long (and short) distances in proteins," *Proceedings of the National Academy of Sciences*, vol. 98, no. 17, pp. 9517–9520, 2001.

[53] T. Uyeda, P. D. Abramson, and J. A. Spudich, "The neck region of the myosin motor domain acts as a lever arm to generate movement," *Proceedings of the National Academy of Sciences*, vol. 93, no. 9, pp. 4459–4464, 1996.

[54] I. Schwaiger, C. Sattler, D. R. Hostetter, and M. Rief, "The myosin coiled-coil is a truly elastic protein structure," *Nature materials*, vol. 1, no. 4, pp. 232–235, 2002.

[55] S. Hvidt, F. H. M. Nestler, M. L. Greaser, and J. D. Ferry, "Flexibility of myosin rod determined from dilute solution viscoelastic measurements," *Biochemistry*, vol. 21, no. 17, pp. 4064–4073, 1982.

[56] T. D. Pollard and G. G. Borisy, "Cellular motility driven by assembly and disassembly of actin filaments," *Cell*, vol. 112, no. 4, pp. 453–465, 2003.

[57] D. Sept, J. Xu, T. D. Pollard, and J. Andrew McCammon, "Annealing accounts for the length of actin filaments formed by spontaneous polymerization," *Biophysical journal*, vol. 77, no. 6, pp. 2911–2919, 1999.

[58] H. Isambert, P. Venier, A. C. Maggs, A. Fattoum, R. Kassab, D. Pantaloni, and M.-F. Carlier, "Flexibility of actin filaments derived from thermal fluctuations. effect of bound nucleotide, phalloidin, and muscle regulatory proteins," *Journal of Biological Chemistry*, vol. 270, no. 19, pp. 11 437–11 444, 1995.

[59] C. P. Brangwynne, G. H. Koenderink, E. Barry, Z. Dogic, F. C. MacKintosh,

and D. A. Weitz, "Bending dynamics of fluctuating biopolymers probed by automated high-resolution filament tracking," *Biophysical journal*, vol. 93, no. 1, pp. 346–359, 2007.

[60] A. Ott, M. Magnasco, A. Simon, and A. Libchaber, "Measurement of the persistence length of polymerized actin using fluorescence microscopy," *Phys. Rev. E*, vol. 48, no. 3, pp. R1642–R1645, 1993.

[61] M. Gardel, J. Shin, F. MacKintosh, L. Mahadevan, P. Matsudaira, and D. Weitz, "Elastic behavior of cross-linked and bundled actin networks," *Science*, vol. 304, no. 5675, pp. 1301–1305, 2004.

[62] C. S. Peskin, G. M. Odell, and G. F. Oster, "Cellular motions and thermal fluctuations: the brownian ratchet," *Biophysical Journal*, vol. 65, no. 1, pp. 316–324, 1993.

[63] A. Mogilner and G. Oster, "Cell motility driven by actin polymerization," *Biophysical journal*, vol. 71, no. 6, pp. 3030–3045, 1996.

[64] W. Cao, J. P. Goodarzi, and E. M. De La Cruz, "Energetics and kinetics of cooperative cofilin–actin filament interactions," *Journal of molecular biology*, vol. 361, no. 2, pp. 257–267, 2006.

[65] B. R. McCullough, L. Blanchoin, J.-L. Martiel, and E. M. De La Cruz, "Cofilin

increases the bending flexibility of actin filaments: implications for severing and cell mechanics," *Journal of molecular biology*, vol. 381, no. 3, pp. 550–558, 2008.

[66] T. D. Pollard, L. Blanchoin, and R. D. Mullins, "Molecular mechanisms controlling actin filament dynamics in nonmuscle cells," *Annual review of biophysics and biomolecular structure*, vol. 29, no. 1, pp. 545–576, 2000.

[67] K. M. Schmoller, T. Niedermayer, C. Zensen, C. Wurm, and A. R. Bausch, "Fragmentation is crucial for the steady-state dynamics of actin filaments," *Biophysical journal*, vol. 101, no. 4, pp. 803–808, 2011.

[68] J. Liu, Y. Sun, G. F. Oster, and D. G. Drubin, "Mechanochemical crosstalk during endocytic vesicle formation," *Current opinion in cell biology*, vol. 22, no. 1, pp. 36–43, 2010.

[69] C. T. Skau and D. R. Kovar, "Fimbrin and tropomyosin competition regulates endocytosis and cytokinesis kinetics in fission yeast," *Current Biology*, vol. 20, no. 16, pp. 1415–1422, 2010.

[70] R. J. Pelham and F. Chang, "Actin dynamics in the contractile ring during cytokinesis in fission yeast," *Nature*, vol. 419, no. 6902, pp. 82–86, 2002.

[71] A. Mogilner and G. Oster, "Polymer motors: pushing out the front and pulling up the back," *Current biology*, vol. 13, no. 18, pp. R721–R733, 2003.

[72] M. F. Fournier, R. Sauser, D. Ambrosi, J.-J. Meister, and A. B. Verkhovsky,

"Force transmission in migrating cells," *The Journal of cell biology*, vol. 188, no. 2, pp. 287–297, 2010.

[73] S. Walcott and S. X. Sun, "A mechanical model of actin stress fiber formation and substrate elasticity sensing in adherent cells," *Proceedings of the National Academy of Sciences*, vol. 107, no. 17, pp. 7757–7762, 2010.

[74] V. E. Galkin, A. Orlova, and E. H. Egelman, "Actin filaments as tension sensors," *Current Biology*, vol. 22, no. 3, pp. R96–R101, 2012.

[75] H. P. Erickson, "Co-operativity in protein-protein association: The structure and stability of the actin filament," *Journal of molecular biology*, vol. 206, no. 3, pp. 465–474, 1989.

[76] R. Cooke, "Role of the bound nucleotide in the polymerization of actin," *Biochemistry*, vol. 14, no. 14, pp. 3250–3256, 1975.

[77] T. Splettstoesser, K. C. Holmes, F. Noé, and J. C. Smith, "Structural modeling and molecular dynamics simulation of the actin filament," *Proteins: Structure, Function, and Bioinformatics*, vol. 79, no. 7, pp. 2033–2043, 2011.

[78] T. Oda, M. Iwasa, T. Aihara, Y. Maéda, and A. Narita, "The nature of the globular-to fibrous-actin transition," *Nature*, vol. 457, no. 7228, pp. 441–445, 2009.

[79] T. Fujii, A. H. Iwane, T. Yanagida, and K. Namba, "Direct visualization of

secondary structures of f-actin by electron cryomicroscopy," *Nature*, vol. 467, no. 7316, pp. 724–728, 2010.

[80] V. E. Galkin, A. Orlova, G. F. Schröder, and E. H. Egelman, "Structural polymorphism in f-actin," *Nature structural & molecular biology*, vol. 17, no. 11, pp. 1318–1323, 2010.

[81] H. Hirata, H. Tatsumi, and M. Sokabe, "Dynamics of actin filaments during tension-dependent formation of actin bundles," *Biochimica et Biophysica Acta (BBA)-General Subjects*, vol. 1770, no. 8, pp. 1115–1127, 2007.

[82] G. W. Greene, T. H. Anderson, H. Zeng, B. Zappone, and J. N. Israelachvili, "Force amplification response of actin filaments under confined compression," *Proceedings of the National Academy of Sciences*, vol. 106, no. 2, pp. 445–449, 2009.

[83] J.-W. Chu and G. A. Voth, "Coarse-grained modeling of the actin filament derived from atomistic-scale simulations," *Biophysical journal*, vol. 90, no. 5, pp. 1572–1582, 2006.

[84] J. Pfaendtner, E. Lyman, T. D. Pollard, and G. A. Voth, "Structure and dynamics of the actin filament," *Journal of molecular biology*, vol. 396, no. 2, pp. 252–263, 2010.

[85] H. Kojima, A. Ishijima, and T. Yanagida, "Direct measurement of stiffness of

single actin filaments with and without tropomyosin by in vitro nanomanipulation," *Proceedings of the National Academy of Sciences*, vol. 91, no. 26, pp. 12 962–12 966, 1994.

[86] P. A. Janmey, S. Hvidt, G. F. Oster, J. Lamb, T. P. Stossel, and J. H. Hartwig, "Effect of atp on actin filament stiffness," *Nature*, vol. 347, pp. 95–99, 1990.

[87] J. Y. Lee, T. M. Iverson, and R. I. Dima, "Molecular investigations into the mechanics of actin in different nucleotide states," *The Journal of Physical Chemistry B*, vol. 115, no. 1, pp. 186–195, 2010.

[88] J.-W. Chu and G. A. Voth, "Allostery of actin filaments: molecular dynamics simulations and coarse-grained analysis," *Proceedings of the National Academy of Sciences of the United States of America*, vol. 102, no. 37, pp. 13 111–13 116, 2005.

[89] E. M. De La Cruz, J. Roland, B. R. McCullough, L. Blanchoin, and J.-L. Martiel, "Origin of twist-bend coupling in actin filaments," *Biophysical journal*, vol. 99, no. 6, pp. 1852–1860, 2010.

[90] T. M. Svitkina and G. G. Borisy, "Arp2/3 complex and actin depolymerizing factor/cofilin in dendritic organization and treadmilling of actin filament array in lamellipodia," *The Journal of cell biology*, vol. 145, no. 5, pp. 1009–1026, 1999.

[91] T. D. Pollard and J. A. Cooper, "Actin and actin-binding proteins. a critical evaluation of mechanisms and functions," *Annual review of biochemistry*, vol. 55, no. 1, pp. 987–1035, 1986.

[92] A. McGough, B. Pope, W. Chiu, and A. Weeds, "Cofilin changes the twist of f-actin: implications for actin filament dynamics and cellular function," *The Journal of cell biology*, vol. 138, no. 4, pp. 771–781, 1997.

[93] J. Pfaendtner, M. Enrique, and G. A. Voth, "Actin filament remodeling by actin depolymerization factor/cofilin," *Proceedings of the National Academy of Sciences*, vol. 107, no. 16, pp. 7299–7304, 2010.

[94] C. Suarez, J. Roland, R. Boujemaa-Paterski, H. Kang, B. R. McCullough, A.-C. Reymann, C. Guérin, J.-L. Martiel, E. M. De La Cruz, and L. Blanchoin, "Cofilin tunes the nucleotide state of actin filaments and severs at bare and decorated segment boundaries," *Current Biology*, vol. 21, no. 10, pp. 862–868, 2011.

[95] E. M. De La Cruz, "How cofilin severs an actin filament," *Biophysical reviews*, vol. 1, no. 2, pp. 51–59, 2009.

[96] E. D. Goley and M. D. Welch, "The arp2/3 complex: an actin nucleator comes of age," *Nature reviews Molecular cell biology*, vol. 7, no. 10, pp. 713–726, 2006.

[97] V. I. Risca, E. B. Wang, O. Chaudhuri, J. J. Chia, P. L. Geissler, and D. A.

Fletcher, "Actin filament curvature biases branching direction," *Proceedings of the National Academy of Sciences*, vol. 109, no. 8, pp. 2913–2918, 2012.

[98] E. Atilgan, D. Wirtz, and S. X. Sun, "Mechanics and dynamics of actin-driven thin membrane protrusions," *Biophysical journal*, vol. 90, no. 1, pp. 65–76, 2006.

[99] E. Atilgan, D. Wirtz, and S. Sun, "Morphology of the lamellipodium and organization of actin filaments at the leading edge of crawling cells," *Biophysical journal*, vol. 89, no. 5, pp. 3589–3602, 2005.

[100] A. A. Halavatyi, P. V. Nazarov, S. Medves, M. Van Troys, C. Ampe, M. Yatskou, and E. Friederich, "An integrative simulation model linking major biochemical reactions of actin-polymerization to structural properties of actin filaments," *Biophysical chemistry*, vol. 140, no. 1, pp. 24–34, 2009.

[101] J. Berro, V. Sirotkin, and T. D. Pollard, "Mathematical modeling of endocytic actin patch kinetics in fission yeast: disassembly requires release of actin filament fragments," *Molecular biology of the cell*, vol. 21, no. 16, pp. 2905–2915, 2010.

[102] D. Vavylonis, Q. Yang, and B. O'Shaughnessy, "Actin polymerization kinetics, cap structure, and fluctuations," *Proceedings of the National Academy of Sciences of the United States of America*, vol. 102, no. 24, pp. 8543–8548, 2005.

[103] M. A. Deriu, A. Shkurti, G. Paciello, T. C. Bidone, U. Morbiducci, E. Ficarra, A. Audenino, and A. Acquaviva, "Multiscale modeling of cellular actin filaments: From atomistic molecular to coarse-grained dynamics," *Proteins: Structure, Function, and Bioinformatics*, vol. 80, no. 6, pp. 1598–1609, 2012.

[104] A. V. Sinitskiy, M. G. Saunders, and G. A. Voth, "Optimal number of coarse-grained sites in different components of large biomolecular complexes," *The Journal of Physical Chemistry B*, vol. 116, no. 29, pp. 8363–8374, 2012.

[105] D. Ming, Y. Kong, Y. Wu, and J. Ma, "Simulation of f-actin filaments of several microns," *Biophysical journal*, vol. 85, no. 1, pp. 27–35, 2003.

[106] J. Berro, A. Michelot, L. Blanchoin, D. R. Kovar, and J.-L. Martiel, "Attachment conditions control actin filament buckling and the production of forces," *Biophysical journal*, vol. 92, no. 7, pp. 2546–2558, 2007.

[107] B. R. McCullough, E. E. Grintsevich, C. K. Chen, H. Kang, A. L. Hutchison, A. Henn, W. Cao, C. Suarez, J.-L. Martiel, L. Blanchoin *et al.*, "Cofilin-linked changes in actin filament flexibility promote severing," *Biophysical journal*, vol. 101, no. 1, pp. 151–159, 2011.

[108] S. Asakura, M. Taniguchi, and F. Oosawa, "Mechano-chemical behaviour of f-actin," *Journal of Molecular Biology*, vol. 7, no. 1, pp. 55–69, 1963.

[109] J. Howard, "Mechanics of motor proteins and the cytoskeleton," 2001.

[110] G. Lan and S. X. Sun, "Flexible light-chain and helical structure of f-actin explain the movement and step size of myosin-vi," *Biophysical journal*, vol. 91, no. 11, pp. 4002–4013, 2006.

[111] G. Lan, P. Sartori, S. Neumann, V. Sourjik, and Y. Tu, "The energy-speed-accuracy trade-off in sensory adaptation," *Nature physics*, 2012.

[112] G. Lan and S. Sun, "Dynamics of myosin-driven skeletal muscle contraction: I. steady-state force generation," *Biophysical journal*, vol. 88, no. 6, pp. 4107–4117, 2005.

[113] G. Lan and S. X. Sun, "Dynamics of myosin-v processivity," *Biophysical journal*, vol. 88, no. 2, pp. 999–1008, 2005.

[114] Z. Wu, V. Elgart, H. Qian, and J. Xing, "Amplification and detection of single-molecule conformational fluctuation through a protein interaction network with bimodal distributions," *The Journal of Physical Chemistry B*, vol. 113, no. 36, pp. 12 375–12 381, 2009.

[115] C. Veigel, F. Wang, M. L. Bartoo, J. R. Sellers, and J. E. Molloy, "The gated gait of the processive molecular motor, myosin v," *Nature cell biology*, vol. 4, no. 1, pp. 59–65, 2001.

[116] M. F. Schmid, M. B. Sherman, P. Matsudaira, and W. Chiu, "Structure of the acrosomal bundle," *Nature*, vol. 431, no. 7004, pp. 104–107, 2004.

[117] V. E. Galkin, A. Orlova, N. Lukoyanova, W. Wriggers, and E. H. Egelman, "Actin depolymerizing factor stabilizes an existing state of f-actin and can change the tilt of f-actin subunits," *The Journal of cell biology*, vol. 153, no. 1, pp. 75–86, 2001.

[118] O. Chaudhuri, S. H. Parekh, and D. A. Fletcher, "Reversible stress softening of actin networks," *Nature*, vol. 445, no. 7125, pp. 295–298, 2007.

[119] O. N. Yogurtcu, J. S. Kim, and S. X. Sun, "A mechanochemical model of actin filaments," *Biophysical Journal*, vol. 103, no. 4, pp. 719–727, 2012.

[120] Y. Arai, R. Yasuda, K.-i. Akashi, Y. Harada, H. Miyata, K. Kinosita, and H. Itoh, "Tying a molecular knot with optical tweezers," *Nature*, vol. 399, no. 6735, pp. 446–448, 1999.

[121] E. M. Craig, D. Van Goor, P. Forscher, and A. Mogilner, "Membrane tension, myosin force, and actin turnover maintain actin treadmill in the nerve growth cone," *Biophysical journal*, vol. 102, no. 7, pp. 1503–1513, 2012.

Vita

Osman N. Yogurtcu began his career in science as an undergraduate at Koc University, Turkey using computational polymer models to study protein-drug interactions. He received his M.Sc. in computational science and engineering from the same institution. During his Ph.D. in the Mechanical Engineering Department at the Johns Hopkins University, his research focused on mechanical properties of biofilaments, such as actin, that have crucial importance on cell viability. At Johns Hopkins, as a mentor in the Graduate Representative Organization (GRO) GradNet Mentoring Program, he helped the incoming graduate students orient themselves to a new campus setting.